www.sciencemag.org/content/350/6256/72/suppl/DC1

Supplementary Materials for

Megasupramolecules for safer, cleaner fuel by end association of long telechelic polymers

Ming-Hsin Wei, Boyu Li, R. L. Ameri David, Simon C. Jones, Virendra Sarohia, Joel A. Schmitigal, Julia A. Kornfield*

*Corresponding author. E-mail: jakornfield@cheme.caltech.edu

Published 2 October 2015, *Science* **350**, 72 (2015)
DOI: 10.1126/science.aab0642

This PDF file includes:

Other supplementary material for this manuscript includes the following:

Materials and Methods

Materials

All chemical reagents were obtained at 99% purity from Sigma-Aldrich, Alfa Aesar, or Mallinckrodt Chemicals. Magnesol ® XL was purchased from The Dallas Group of America, Inc. ^{1}H-NMR spectra were obtained using a Varian Inova 500 spectrometer (500 MHz); all spectra were recorded in $CDCl_3$. Chemical shifts were reported in parts per million (ppm) and were referenced to residual protio-solvent resonances. Deuterated solvents used for ^{1}H-NMR and SANS experiments ($CDCl_3$ and d_{12}-cyclohexane) were purchased from Cambridge Isotope Laboratories. Cylindrical quartz "banjo" cells used in scattering experiments were purchased from Hellma Analytics.

Representative procedure for purification of COD

Redistilled-grade COD (72.3 g, 0.67 mol) was syringe-transferred to a 250 ml Schlenk flask in an ice bath under argon. 1 M BH_3·THF complex in THF (108 ml, 0.11 mol) was slowly added into the flask over 10 min. The flask was taken out of the ice bath, and left to stir under argon at room temperature for 2 h. THF was evaporated under reduced pressure at room temperature to an extent that the concentration of residual THF in the mixture was below 300 ppm (verified by ^{1}H NMR analysis). The monomer was vacuum distilled from the mixture at 40°C into a 100 ml Schlenk flask (loaded with 9 g of Magnesol® XL and a stir bar) in a dry-ice tub. The mixture was stirred under argon atmosphere at room temperature overnight. The monomer was vacuum distilled from the mixture into a 100 ml Schlenk flask (loaded with 10 g of calcium hydride (CaH_2) and a stir bar) in a dry-ice tub. After stirring at room temperature for 3 h under argon flow, the monomer was vacuum distilled from the mixture into a 100 ml Schlenk flask in a dry-ice tub. After being warmed to ambient temperature, the flask was sealed with a Suba-Seal rubber septum while argon was flowing through the flask, and placed in a freezer at -30°C for storage of the rigorously purified COD (40.0 g, 55.3% yield). The rigorously purified monomer was vacuum distilled again prior to use.

Representative procedure for synthesis of non-associative telechelic polycyclooctadienes of M_w > 400 kg/mol by two-step ROMP

Di(di-*tert*-butyl-isophthalate)-terminated CTA (6.5 mg, 4.58 μmol) was placed in a 50 ml Schlenk flask, and degassed by 5 cycles of pulling vacuum/filling argon. Degassed, anhydrous DCM (0.5 ml) was syringe-transferred into the flask to dissolve the CTA. 0.13 ml of 1 mg/ml anhydrous DCM solution of Grubbs II (0.13 mg, 0.16 μmol) was injected into the mixture to equilibrate with the CTA, followed immediately by the addition of a small amount of degassed, freshly vacuum-distilled rigorously purified COD (0.03 g, 0.23 mmol) to the mixture to start the polymerization reaction. The mixture was stirred at 40°C for 1 h. Another 0.13 ml of freshly prepared 1mg/ml DCM solution of Grubbs II was injected, followed by a large amount of freshly vacuum-distilled, rigorously purified COD (5.00 g, 45.8 mmol) in degassed, anhydrous DCM (12 ml). The mixture was stirred at 40°C for 4-10 min. The reaction was stopped by exposure to air, and additional DCM (30 ml) + 0.1 g of BHT were added. The diluted mixture was precipitated into 400 ml of acetone at room temperature. The precipitated polymer was collected and dried under reduced pressure at room temperature overnight. Polymers with designed molar mass and PDI around 1.5 were obtained.

GPC-MALLS

MALLS was used in conjunction with GPC to determine the molecular weights and polydispersity of the polymers. Our system used a Wyatt DAWN EOS multi-angle laser light scattering detector (λ=690nm) with a Waters 410 differential refractometer (RI) (λ=930nm) connected in series. Chromatographic separation by the size exclusion principle (largest comes out first) was achieved by using four Agilent PLgel columns (pore sizes 10^3,10^4,10^5, and 10^6 Å) connected in series. Degassed THF was used as the mobile phase with a temperature of 35°C and a flow rate of 0.9ml/min. The time for complete elution through the system was 50 min, and MALLS and RI data were recorded at 5Hz. Samples were prepared by dissolving 5mg of polymer in 1ml of THF and filtering the solution through 0.45µm PTFE membrane syringe filters immediately before injection. An injection volume of 20µl was used. The data were analyzed by Wyatt Astra Software (version 5.3.4) using the Zimm fitting formula with *dn/dc* = 0.125 for PCOD in THF to obtain weight-average molecular weight (M_w) for each polymer reported. Polymers are described in the table S1.

Table S1: Characterization of polymers in this paper. ([a]: determined by GPC-MALLS in THF; [b]: determined by batch-mode MALLS in cyclohexane.)

Polymer	M_w[a] (kg/mol)	M_n[a] (kg/mol)	PDI[a]	M_w[b] (kg/mol)
45kNA	48.5	31.3	1.55	
45kDA	44.7	28.6	1.56	
45kDB	48.8	36.7	1.33	
140kNA	138.5	89.8	1.54	
140kDA	143.1	90.2	1.59	
140kDB	148.0	100.0	1.48	
300kNA	318.4	213.5	1.49	
300kDA	304.3	201.3	1.51	
300kDB	290.1	198.3	1.46	320±20
670kNA	637.5	441.0	1.45	
670kDA	671.4	445.5	1.51	
670kDB	629.2	436.2	1.44	600±50
76kNA	76.2	52.3	1.46	
76kTA	91.2	57.0	1.60	
230kNA	232.8	155.4	1.50	
230kTA	374.5	218.7	1.71	
430kNA	430.0	288.6	1.49	
430kTA	510.0	316.8	1.61	

Rheology

Polymers were dissolved by shaking with tetralin, cyclohexane or Jet-A. To confirm that the end-association among telechelics is responsible for the changes in fluid properties, additional controls were prepared by treating some associative telechelic solutions (1.76 mg/ml) with 2.5

μl/ml triethylamine (TEA) to block their end association. Shear-flow rheology data were obtained at 25°C with stress-controlled rheometer TA AR1000, equipped with a cone-plate geometry (angle 1°, diameter 60 mm) for polymer solutions in tetralin and Jet-A, and a strain-controlled rheometer TA ARES-RFS, equipped with a cone-plate geometry (angle 2°, diameter 50mm) and a solvent trap for polymer solutions in cyclohexane, with shear rate ranging from 1000 s^{-1} to 10 s^{-1}. For polymer solutions in tetralin, we checked that the viscosities measured by AR1000 and ARES-RFS agreed with each other well. The specific viscosity values shown in Fig. 2 were averaged over data points taken from the range that doesn't have shear rate dependence (e.g., the range is 300 to 10 s^{-1} in Fig. 3a 'DA/DB'). Three replicates with freshly prepared solutions were measured to obtain the error bars (SD values).

SANS

d_{12}-Cyclohexane solutions of polymers were prepared by weighing out polymer on a Mettler precision balance (±0.01mg) into new glass scintillation vials with PTFE lined caps and subsequently adding the appropriate amount of solvent using a precision syringe (±1%). These were subsequently placed on a wrist action shaker at room temperature overnight.
SANS data in the paper were obtained at the National Institute of Standards and Technology (NIST) on beamline NG-3, preliminary experiments (data not shown) were conducted at Oak Ridge National Laboratory (ORNL) on beamline CG-2 at the High Flux Isotope Reactor (HFIR). Samples were placed in Hellma quartz cylindrical cells with 5mm path length. Temperature was controlled by a recirculating water bath at NIST and by Peltier at ORNL. All scattering experiments were conducted at 25°C. Two-dimensional scattering patterns were taken for each sample using three detector distances (1.3-13 m at NIST and 0.3-18.5m at ORNL). The overall scattering vector ranges were $0.003 < q(Å^{-1}) < 0.4$ at NIST and $0.002 < q(Å^{-1}) < 0.8$ at ORNL with the effective limits for a given sample determined by the signal to noise ratio.

MALLS ("batch mode")

MALLS (not connected to GPC) was used to characterize the supramolecular assembly behavior of complementary associative telechelic polymers (DA/DB mixtures) in cyclohexane. Cyclohexane solutions of polymers were prepared by weighing out polymer on a Mettler precision balance (±0.01mg) into new glass scintillation vials (20 ml) with metal foil lined caps and subsequently adding the appropriate amount of solvent using a precision syringe (±1%). These were subsequently placed on a wrist action shaker at room temperature overnight. All solutions were filtered through 0.45 μm PTFE filters into clean glass scintillation vials (20 ml) and allowed to equilibrate for at least 24 hours prior to characterization. MALLS measurements were carried out using a Wyatt DAWN EOS laser light scattering instrument in "batch mode" with 18 detectors in the angular range from 22.5 to 147° using a solid-state laser (λ=690nm). Data were acquired at 35 °C three times (rotating the vial to average out heterogeneities) for at least 2 minutes and analyzed using Wyatt Astra Software (version 5.3.4). The associative supramolecules conformed to the Zimm fitting formula, which was used to evaluate the apparent weight-average molecular weight (app M_w) and apparent radius of gyration (app R_g) for each polymer composition at each concentration, with dn/dc = 0.11 for PCOD in cyclohexane.

Modeling

Here we identify a set of parameter values for which the equilibrium distribution of the supramolecular species is suitable for mist-control applications. Based on prior literature on ultra-long polymers (which themselves are not acceptable due to shear degradation during routine handling of fuel and incompatibility with engine systems), polyisobutylene chains having weight-average molecular weight ~5×10^6 g/mol are satisfactory mist-suppressing agents at concentrations as low as 50 ppm in kerosene (*2*). Therefore, we use a theoretical model of ring-chain equilibrium to identify choices of the molecular weight of telechelic chains (MW_p), the strength of end-association (εkT) and concentration (ϕ_{total}) that would provide 50 ppm of "mega-supramolecules" (linear supramolecules of $M_w \geq 5\times10^6$ g/mol and cycles of $M_w \geq 10\times10^6$ g/mol). We begin with the results that motivated us to synthesize exceptionally long telechelics and guided the selection of associative end groups: the model indicates that chains of approximately 5×10^5 g/mol to 1×10^6 g/mol with ends that associate with strength $16kT - 18kT$ at approximately 800-1400ppm concentration could provide the necessary concentration of mega-supramolecules. Details of the particular theoretical formulation that we developed are given in the second half of this supplement.

1. RING-CHAIN EQUILIBRIUM OF LONG, END-ASSOCIATIVE TELECHELICS

1.1. Parameter Space

Results are presented for complementary pairs of telechelic polymers (A----A, B----B) that have similar backbone lengths ($MW_A = MW_B = MW_p$) in stoichiometric solutions ($\phi_{Atotal} = \phi_{Btotal} = \phi_{total}/2$). When the A and B end-groups meet, they form a physical association with energy ε. In the resulting parameter space of $\{MW_p, \varepsilon, \phi_{total}\}$, we seek to optimize the equilibrium distribution of supramolecules for mist-control applications, within the constraints on MW_p ($M_w \leq 1\times10^6$ g/mol) and ϕ_{total} (< 5,000 ppm) in the context of fuel additives.

The challenge associated with using end-to-end association at the low concentrations relevant to fuel is the tendency to form small cyclic species that, in effect, consume most of the telechelic building blocks without contributing to mist control. To reduce the fraction of telechelic chains incorporated into cyclic species, we use very long telechelics, which reduce the fraction of polymer "wasted" in small rings because the loop closure probability scales as $N^{-3/2}$ for Gaussian

chains and $N^{-1.66}$ for swollen chains (see §2). Based on prior literature on shear degradation, we consider MW_p = 1×10^6 g/mol as our upper bound and compare it to chains that are half that length MW_p = 0.5×10^6 g/mol to quantify sensitivity to MW_p. As a further step to mitigate formation of small rings, we use complementary association of A----A and B----B telechelics, for which the smallest ring is a dimer. This reduces the amount of telechelic wasted in small cyclics due to two effects: i) the entropy penalty for ring closure for the smallest possible ring is much greater than the penalty for closing a ring of size a single telechelic because the loop is twice as long as a single telechelic; and ii) the odd rings (cycles of 1, 3, 5,… telechelics) are eliminated, greatly reducing the fraction of building blocks partitioned in cyclic species.

Another challenge in the context of fuel additives is the need to maintain low viscosity. The longer a polymer is, the lower the concentration ϕ^* at which the chains begin to overlap and viscosity begins to increase strongly. Therefore, the total polymer concentration ϕ_{total} needs to be less than the overlap concentration of the individual telechelic building blocks, $\phi^*(MW_p)$. Further, the model shows that a concentration of ϕ_{total} = ¼ $\phi^*(MW_p)$ is low enough that all supramolecules in the equilibrium distribution are below their respective overlap concentrations. For the two chain lengths selected above, results are presented for ϕ_{total} = ¼ $\phi^*(MW_p)$, which is 800 ppm for MW_p = 1×10^6 g/mol, and 1400 ppm for MW_p = 0.5×10^6 g/mol. In addition, results are presented for 1×10^6 g/mol at 1400 ppm, both to illustrate the change in the distribution of supramolecular species with increasing concentration (from ϕ_{total} = 800ppm to 1400ppm for MW_p = 1×10^6 g/mol) and to illustrate the effect of the size of the telechelic building blocks at matched total concentration (comparing both chain lengths at ϕ_{total} = 1400ppm). With the above choices for MW_p and ϕ_{total}, the problem is reduced to a single dimension, ε, which is examined over its physically relevant range: it must be much greater than kT to drive association and it must be much less than 150kT (approximate strength of a covalent bond) so that the reversible links can function as tension relief links that protect against chain scission in strong flows.

Table S2: Literature Values for Parameters in the Model

Polydiene 1,4-rich	backbone double cis	backbone double trans	non-1,4-units (b)	ρ [g/ml]	C∞	b [nm]	M_K [g/mol]	References
Polyisoprene	100% (a)	0 (a)	0 (a)	0.910	5.2	0.93	128.6	*31*
	70%	23%	7%	0.900	4.7	0.84	119.6	*32*
	19%	45%	36%	0.895	5.3	0.96	156.9	*31,33*
Polybutadiene	98%	1%	1%	0.900	4.6	0.83	90.5	*31,34*
	29%	53%	18%	0.895	5.6	1.01	119.8	*31,35*
	44%	59%	7%	0.895	5.5	0.99	112.5	*31,35*

Properties measured at temperature of 25°C.

ρ	density in the melt state
C∞	characteristic ratio
b	Kuhn step length
M_K	molar mass of a Kuhn segment

Shaded cells: most similar to the polycyclooctadiene in this study, which has 75% cis units, 25% trans units and no 1,4-units.

Notes:
(a) natural rubber
(b) for polyisoprene, these are mainly 3,4-units and trace amounts of 1,2-units; and for polybutadiene, these are 1,2-units

1.2. Computational Results and Relationship to Experiment

To guide the design of an experimental system, we consider the relationship of model parameters to polymers having unsaturated hydrocarbon backbones—1,4-polyisoprene (PI), 1,4-polybutadiene (PB) and polycyclooctadiene (PCOD)—in Jet-A solvent. The model is formulated with sites of volume a^3 on a lattice with coordination number $c = 6$. The lattice size $a^3 = v_K$, where $v_K = MW_K/(\mathcal{N}_A\rho)$ is the volume of a Kuhn segment (with $\mathcal{N}_A$ denoting Avogadro's number and ρ, the polymer density) for a specific polymer of interest. A chain of molecular weight MW_p maps onto $M = MW_p/MW_K$ connected lattice sites. To model a solution at volume fraction ϕ_p, we treat a system of N_p polymer molecules in a volume $V = (MN_p+N_s)a^3$, adjusting the number of solvent lattice sites to give the specified concentration, *i.e.*, $N_s = MN_p(1-\phi_p)/\phi_p$. To quantify the entropic cost of loop closure (§2.2), numerical values are needed for the small end-to-end distance x required to close a loop and for the number of monomers in a thermal blob $g_T \approx b^6/v^2$. For simplicity we choose $x/b = 1$.

All three backbones of interest here, PI, PB and PCOD, can be represented to good approximation by a single set of parameters, because the differences among them are relatively small (table S2). For these unsaturated hydrocarbon backbones, variations in molecular parameters result from differences in cis/trans ratio of the backbone double bonds and the

fraction of monomer insertions that create short side chains (3,4- and 1,2-units in PI and PB). If all six chain microstructures in table S2 are considered, the lattice size is a = 0.61±0.03nm. We focus on polymers that have very few side chains (PCOD does not have any); if only microstructures with ≤7% 3,4- and 1,2-units, the lattice size shifts very slightly to a = 0.59±0.03nm. Similarly, the molecular weight of a Kuhn segment is MW_K = 121±22 g/mol if all six microstructures are included and shifts slightly to MW_K = 113±16 g/mol if we exclude microstructures with 18% or more 3,4- and 1,2-units. The Kuhn step length is roughly 50% greater than the lattice size a: if all six microstructures are included b = 0.93±0.07nm (with ≤7% 3,4- and 1,2-units, b = 0.90±0.08nm). The excluded volume parameter v was estimated as $v/b^3 \approx$ 0.10 for PI in Jet-A, consistent with $g_T \approx 100$. (*36*) Based on literature results in cyclohexane, the expanded conformations of PI and PB are very similar when they are dissolved in a good solvent that is similar to Jet-A (R_g [nm] = $A(MW)^{\nu}$, with A = 0.0129 for PB and 0.0126 for PI, and with ν = 0.609 for PB and 0.610 for PI). Thus, theoretical predictions with a single set of parameters are expected to provide equally good guidance for molecular design with PI, PB and PCOD backbones. Results are shown for MW_K = 113 g/mol, a = 0.61 nm, b = 0.90 nm, x/b = 1 and g_T = 100

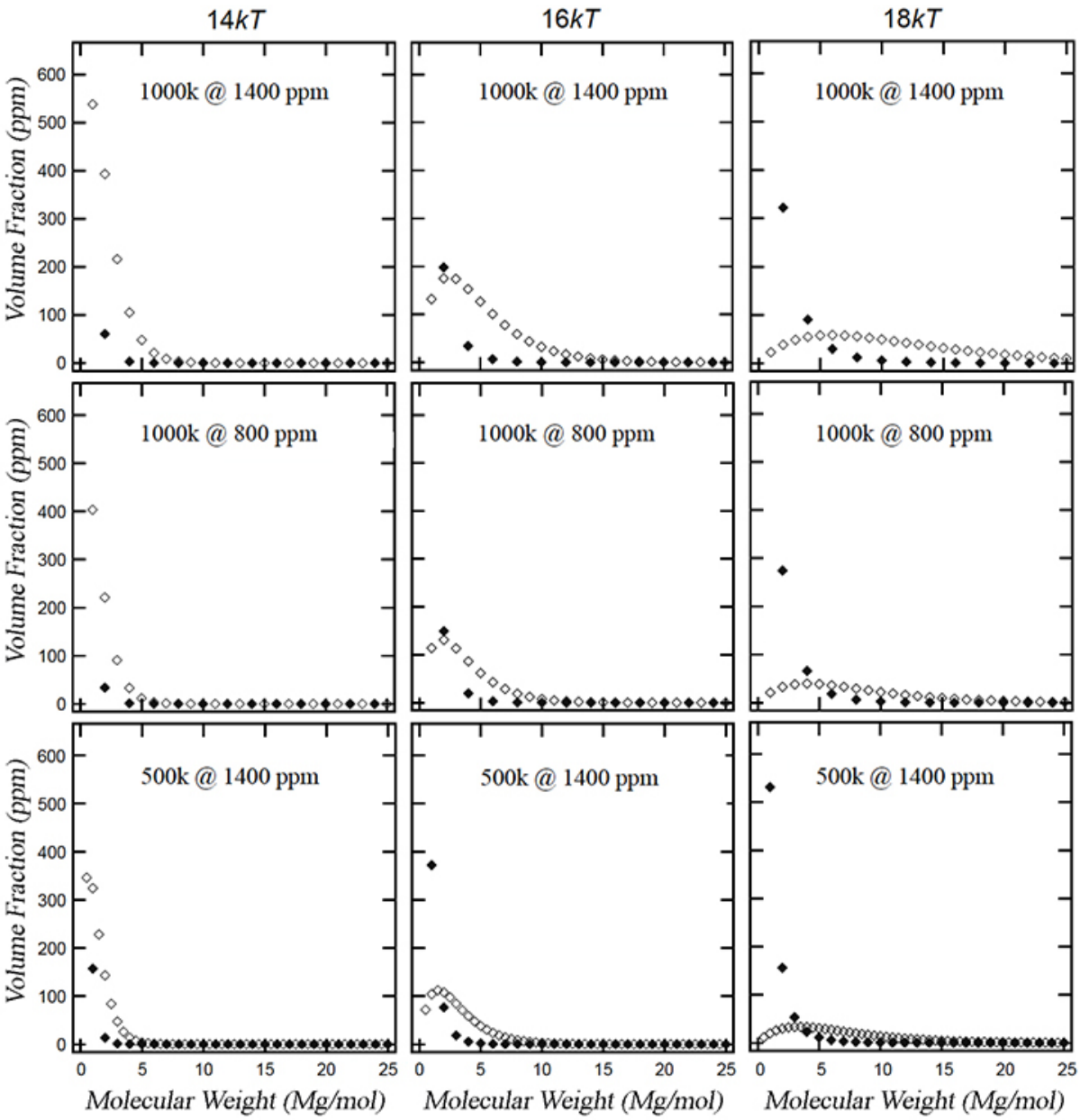

Figure S1 Model predictions for two different values of the strength of interaction $\varepsilon kT = 14kT$ (left), $\varepsilon kT = 16kT$ (middle) and $\varepsilon kT = 18kT$ (right) (open diamond: linear supramolecules; solid diamond: cyclic supramolecules).

The model predicts the equilibrium distribution of aggregates in terms of concentrations of supramolecular species with various sizes as functions of polymer concentration, length of the telechelic building blocks and binding energy. The model could serve as a guideline to achieve the desired rheological benefits (mist control and drag reduction).

- Concentration: Comparison of model results for $MW_p = 10^6$ g/mol (labeled 1000k) at total polymer volume fraction ϕ_{total} of 1400 ppm and 800 ppm (fig. S1) demonstrates two important

effects of total polymer concentration. First, at fixed MW_p and ε, increasing concentration improves the fraction of the polymer involved in larger linear aggregates (compare upper right and middle right in fig. S1): at 1400 ppm the distribution of linear supramolecules (open symbols) decays more gradually with increasing M_W, and the position of the peak in ϕ_{linear} *vs*. M_W is greater at 1400 ppm than at 800 ppm (most visibly for ε=18, right column of fig. S1).

- Length of the telechelic building blocks: Longer chains begin to overlap at a lower concentration than shorter ones. To examine the effect of the length of the individual building blocks (MW_p) at similar degree of overlap, we compare them at ϕ_{total} = ¼ ϕ^* for their respective $\phi^*(MW_p)$: results for 5×10^5 g/mol chains at 1400 ppm (bottom row, fig. S1) and 1×10^6 g/mol chains at 800 ppm (middle row). The shape of the ϕ_{linear} *vs*. M_W does not change significantly with MW_p (for all ε). The important effect of MW_p is that longer telechelics reduce the fraction of polymer "wasted" in rings with small aggregation numbers, due to the increased entropic cost of cyclization for larger loops.
- Energy of association: The equilibrium distribution changes qualitatively as the association energy increases (fig. S1, from left to right): the population of loops of all sizes increases (due to higher penalty for dangling ends) and the breadth of the distribution of linear species broadens and the peak in ϕ_{linear} decreases. At values of $\varepsilon \leq 14$, aggregates are few and the dominant components are the telechelic building blocks themselves. At values of $\varepsilon \geq 20$ (not shown), the dominant components are cycles of low M_W. Intermediate values of the energy of association, corresponding to $16 \leq \varepsilon \leq 18$, provide a balance of interactions strong enough to drive formation of large supramolecules and weak enough to accommodate a significant population of linear superchains (with unpaired ends).

1.3. Implications for Mist-Control Applications

The model showed that optimal formation of "mega-supramolecules" (linear supramolecules of $M_W \geq 5 \times 10^6$ g/mol and cycles of $M_W \geq 10 \times 10^6$ g/mol) correlates with maximizing the equilibrium fraction of polymers involved in linear supramolecules in the 5–10 $\times 10^6$ g/mol range. Two key features of the distributions that satisfy this objective are (i) favorable partitioning of the polymer into linear rather than cyclic supramolecules, and (ii) a well-defined peak in ϕ_{linear} centered around ~ 5×10^6 g/mol. As expected, partitioning of the polymer into linear supramolecules is favored at higher values of MW_p and ϕ_{total}—but both of these quantities

are constrained due to the limitations of shear degradation ($M_W \leq 10^6$ g/mol) and system compatibility for fuel ($\phi_{total} \leq$ ¼ ϕ^*). Near these maximal values, the strong dependence of the supramolecular distributions on the energy of interactions has important implications for mist-control applications. For mixtures of A----A and B----B molecules, model predictions indicate that favorable results will be found in a relatively narrow range of association energy, $16 \leq \varepsilon \leq 18$.

1.4 Time to Reach the Equilibrium Distribution

The model assumes that under conditions of practical importance, equilibrium is restored as fast as it is disturbed. Therefore, we consider the question "How long does it take to reach the equilibrium partitioning of the polymer into aggregates of all sizes?" The average lifetime of a donor-acceptor physical bond is estimated using $\tau_b \sim \tau_0 \exp(\varepsilon)$, where $\tau_0 \sim \eta b^3/kT$ describes a typical motional time for a monomer in solvent with shear viscosity η. For solvents like fuel, $\eta \sim 1$ mPa·s, giving $\tau_0 \sim 10^{-10}$ s, so the lifetime is on the order of $\tau_b \sim$ 1ms for $\varepsilon = 17$. Therefore, if equilibrium could be reached with roughly 10^3 bond-breaking and bond-forming events and for end-groups with 16–18kT energy of association, that time is on the order of 1s.

2. THEORETICAL TREATMENT

While there are already many studies of the theory of ring-chain equilibrium, we were interested in formulating the problem so that we could readily solve the equilibrium population as a function of the length, concentration and association energy. In our construction, terms arising from microscopic interactions, as well as terms arising from the center-of-mass and configurational entropy (except loop closure) of polymer components and solvent in solution are carried out explicitly. Whereas terms arising from (i) the energy of association of the end-groups within a polymer aggregate, and (ii) the entropic cost of loop closure for cyclic supramolecular aggregates are absorbed into the standard chemical potentials of the polymeric species.

As a first step in modeling the equilibrium distribution of cyclic and linear supramolecules from telechelic polymers A----A and B----B (fig. S2), we start with the case of association of telechelic polymers A_1----A_2 and B_1----B_2. Subsequently, we show that the predicted distributions hold for A----A and B----B as well (§2.3). We assume that the end-groups A_1 and

A_2, and likewise B_1 and B_2, are distinguishable but of identical reactivity (as though one end were isotopically labeled).

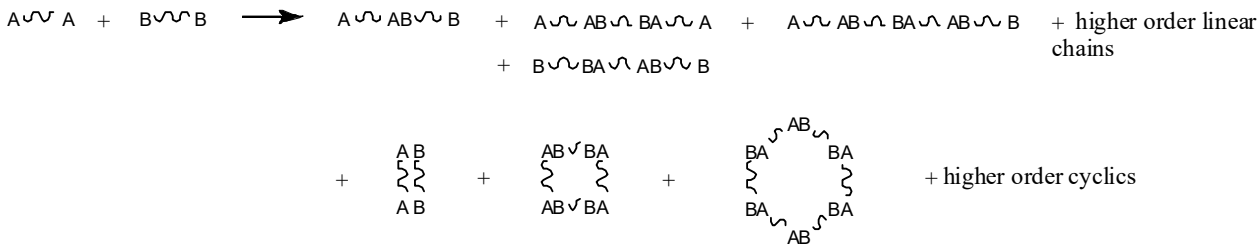

Figure S2 Molecular design for self-assembly of telechelic polymeric building blocks into larger linear and cyclic supramolecules *via* end association

2.1 Model Description

We approximate this equilibrium using a lattice model following Goldstein (*25*). A solution of N_s solvent molecules and N_{Atotal} and N_{Btotal} telechelic A_1----A_2 and B_1----B_2 chains of M_A and M_B repeat units, respectively, occupies a volume V that is partitioned into lattice sites of volume a^3, which is the volume of a solvent molecule and also the volume of a monomer. There is negligible volume change upon mixing, so $V = a^3(N_s + N_{Atotal}M_A + N_{Btotal}M_B) = \Lambda a^3$, where Λ is the total number of "sites." Subscripts i (or j) refer to polymeric components. Component i is composed of n_i A_1----A_2 building blocks and m_i B_1----B_2 building blocks, and has $M_i = n_iM_A + m_iM_B$ repeat units. The volume fraction of solvent is $\phi_s = N_s/\Lambda$ and that of component i is $\phi_i = N_iM_i/\Lambda$. Unless otherwise specified, sums $\sum_i$ are over all polymer components in solution, *e.g.*, the sum of the volume fractions of all polymeric species must equal the total polymer volume fraction $\phi = \sum_i M_iN_i/\Lambda = 1-\phi_s$.

The total free energy F of the solution is the sum of entropic and enthalpic contributions, F_S and F_{int}, and of contributions from the internal free energy of solvent and polymer components:

$$F = F_{int} + F_S + N_s\mu_s^0 + \sum_j N_j\mu_j^0 \qquad (1)$$

where μ_j^0 is the standard chemical potential of polymeric component j. The first term is due to solvent-solvent, polymer-solvent, and polymer-polymer interactions, which are estimated by the random mixing approximation:

$$F_{int} = \Lambda\delta\left[(1-\phi)^2 h_{ss} + \phi^2 h_{pp} + 2\phi(1-\phi)h_{ps}\right] \qquad (2)$$

where δ is one-half the local coordination number, and h_{ij} are the microscopic interaction energies of the polymer and solvent species. The second term is due to configurational and center-of-mass entropy, S:

$$S = k\sum_j \ln \Omega(0, N_j) + \Delta S_{mix} \tag{3}$$

where $\Omega(0,N_j)$ is the number of possible configurations of N_j molecules of polymer component j each having M_j repeat units, onto M_jN_j sites (*i.e.*, pure component j before mixing with other polymer species or solvent). Following the notation of Hill (*37*) for the entropy of a melt of N_i linear polymer chains of length M_i:

$$\ln \Omega(0, N_i) = -N_i \ln N_i + N_i + M_i N_i \ln(M_i N_i) - M_i N_i + N_i(M_i - 1)\ln\left(\frac{c-1}{M_i N_i}\right) \tag{4}$$

where c is the coordination number. The entropy of mixing of the solvent and all polymer components, ΔS_{mix}, is approximated using the Flory-Huggins expression:

$$\Delta S_{mix} = -k\left(N_s \ln \phi_s + \sum_j N_j \ln \phi_j\right). \tag{5}$$

The entropic contribution to the free energy of the mixture is therefore:

$$\begin{aligned} F_S &= -T\Delta S_{mix} - kT\sum_j \ln \Omega(0, N_j) \\ &= kT\left[N_s \ln\left(\frac{N_s}{\Lambda}\right) + \sum_j N_j \ln\left(\frac{N_j}{\Lambda}\right)\right] + kT\sum_j N_j \ln\left(M_j\right) - kT\sum_j \ln \Omega(0, N_j) \end{aligned} \tag{6}$$

where ϕ_s and ϕ_j are replaced by N_s/Λ and N_jM_j/Λ respectively.

The equilibrium distribution of species is readily analyzed in terms of the chemical potentials of the solvent μ_s and the polymeric species μ_i. For example, at equilibrium, the chemical potential of a supramolecular component i made up of n_i A_1----A_2 and m_i B_1----B_2 must satisfy the equilibrium condition:

$$\mu_i = n_i\mu_A + m_i\mu_B \tag{7}$$

where μ_A and μ_B are the chemical potentials of building blocks A_1----A_2 and B_1----B_2, respectively. The chemical potential of polymer component i involves both interactions

(solvent-solvent, polymer-solvent and polymer-polymer) and entropic contributions. The contribution to the chemical potential of component *i* due to *interactions* is:

$$\mu_{int,i} = \left.\frac{\partial F_{int}}{\partial N_i}\right|_{N_{j\neq i}} = -\omega M_i \phi_s^2 + \omega_{pp} M_i \qquad (8)$$

where we have used $\phi = (M_i N_i + \sum_{j\neq i} M_j N_j)/\Lambda$ with $\Lambda = N_s + M_i N_i + \sum_{j\neq i} M_j N_j$ and $\phi_s = 1-\phi$ and, for convenience, have introduced $\omega_{mn} = \delta h_{mn}$ and $\omega = \omega_{pp} + \omega_{ss} - 2\omega_{ps}$. The *entropic* contribution to the chemical potential of component *i* is:

$$\frac{\mu_{S,i}}{kT} = \frac{1}{kT}\left.\frac{\partial F_S}{\partial N_i}\right|_{N_{j\neq i}} = \ln\left(\frac{\phi_i}{M_i}\right) + 1 - \phi_i - M_i\left[\phi_s + \sum_{j\neq i}\frac{\phi_j}{M_j}\right] + \ln M_i \qquad (9)$$
$$-1 - M_i\left[\ln(c-1) - 1\right] - \ln M_i + \ln(c-1)\,.$$

Differentiation of Equation 6 and substitution of Equations 7 and 9 give the following expression for the chemical potential of component *i*, valid for the single-chain building blocks and all supramolecules:

$$\mu_i = \left.\frac{\partial F}{\partial N_i}\right|_{N_{j\neq i}} = \mu_i^0 + kT\left\{\ln\left(\frac{\phi_i}{M_i}\right) - M_i\left[\phi_s + \sum_j \frac{\phi_j}{M_j}\right] + f_i\right\} - \omega M_i \phi_s^2 + \omega_{pp} M_i \qquad (10)$$

where $f_i = \ln(c\text{-}1) + M_i[1\text{-}\ln(c\text{-}1)]$. Substituting the expressions for μ_i, μ_A, and μ_B from Equation 10 into Equation 7 above, we obtain, after rearrangement, the following mass-action relation for component *i*:

$$\mu_i^0 + kT\left[\ln\left(\frac{\phi_i}{M_i}\right) + f_i\right] = n_i\mu_A^0 + m_i\mu_B^0 + kT\left[n_i \ln\left(\frac{\phi_A}{M_A}\right) + m_i \ln\left(\frac{\phi_B}{M_B}\right) + n_i f_A + m_i f_B\right] \qquad (11)$$

where ϕ_A and ϕ_B are the *equilibrium volume fractions* of the free telechelics A_1----A_2 and B_1----B_2, respectively. It is convenient to rewrite Equation 11 as follows:

$$\left(\frac{\phi_i}{n_i M_A + m_i M_B}\right) = \left(\frac{\phi_A}{M_A}\right)^{n_i}\left(\frac{\phi_B}{M_B}\right)^{m_i} \exp(\Gamma_i) \qquad (12)$$

,

where $$\Gamma_i = \frac{1}{kT}(n_i\mu_A^0 + m_i\mu_B^0 - \mu_i^0) + (n_i + m_i - 1)\ln(c-1)\,. \qquad (13)$$

The conservation equations are then:

$$\phi_{Atotal} = \sum_j \phi_j \left(\frac{n_j M_A}{n_j M_A + m_j M_B} \right)$$

$$\phi_{Btotal} = \sum_j \phi_j \left(\frac{m_j M_B}{n_j M_A + m_j M_B} \right)$$

To this point, our formulation has treated terms arising from microscopic interactions, as well as center-of-mass and configurational entropy (except loop closure) of polymer components and solvent. Next we account for (i) the energy of association of the paired end-groups within a supramolecule and (ii) the entropic cost of loop closure for cyclic supramolecules, which we incorporate into the standard chemical potentials μ_j^0.

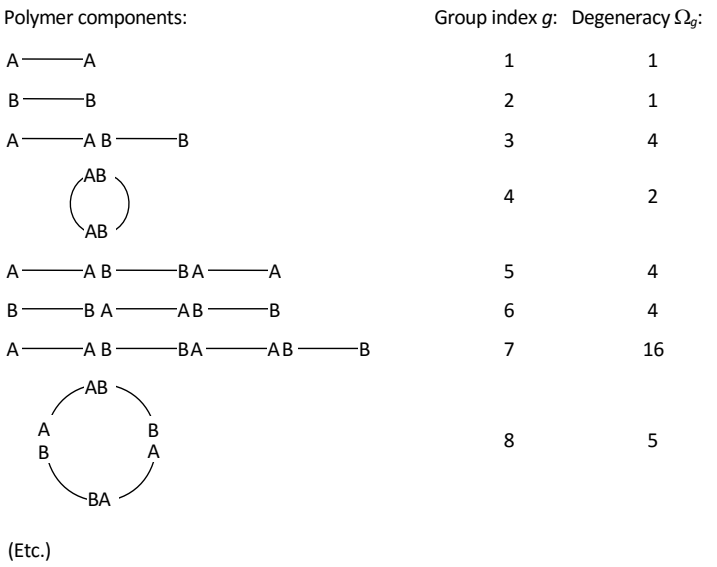

Figure S3 Grouping of polymer components, where A and B generically refer to A1 or A2 and B1 or B2 end-groups. Each group is composed of all the different possible aggregates obtained by the assembly of the A1----A2 and B1----B2 building blocks. For example, group 3 is composed of the following 4 distinct aggregates: A1----A2B1----B2, A1----A2B2----B1, A2----A1B1----B2, and A2----A1B2----B1.

For this purpose, it is useful to identify "groups" of polymer species, each assigned an index g, that are topologically similar and have the same values of $M_j = M_g$, $n_j = n_g$, $m_j = m_g$, and $\Gamma_j = \Gamma_g$. In identifying "groups" of polymer species, A and B are used to refer to A1 or A2 and B1 or B2, respectively (fig. S3). In counting number of distinct species in group g (Ω_g,) we treat the two ends of an A-telechelic or a B-telechelic as distinguishable. Thus, group g is composed of all the different possible aggregates obtained by the assembly of the A1----A2 and B1----B2 building blocks. For example, group g = 3 has Ω_g = 4 distinct aggregates (fig. S3): A1----A2·B1----B2, A1----A2·B2----B1, A2----A1·B1----B2, and A2----A1·B2----B1.

How many components belong to each group? For linear aggregates there are two possibilities: (i) for $n_g + m_g$ even (i.e., $n_g = m_g$), no sequence read from left to right will be the same as a sequence read from right to left, so the number of ways to arrange the molecules is $\Omega_g = 2^{n_g + m_g}$; (ii) for $n_g + m_g$ odd, every sequence read from left to right will have a matching sequence read from right to left, so the number of ways to arrange the molecules is $\Omega_g = 2^{n_g + m_g - 1}$.

Supramolecular cycles always have $n_g = m_g$. The number of ways to form such a loop is derived in §2.3 below; to good approximation it is $\Omega_{cyc,g} = 2 + (2^{2n_g - 1} - 2)/n_g$.

The fact that (by construction) all of the components j in any particular group g have the same value of $\mu_j^0 = \mu_g^0$ allows the equilibrium condition and the conservation equations to be rewritten in terms of ϕ_g, the cumulative volume fraction of all polymer components in group g:

$$\left(\frac{\phi_g}{n_g M_g + m_g M_g}\right) = \Omega_g \left(\frac{\phi_A}{M_A}\right)^{n_g} \left(\frac{\phi_B}{M_B}\right)^{m_g} \exp(\Gamma_g) \tag{15}$$

$$\begin{aligned} \phi_{Atotal} &= \sum_g n_g M_A \Omega_g \left(\frac{\phi_A}{M_A}\right)^{n_g} \left(\frac{\phi_B}{M_B}\right)^{m_g} \exp(\Gamma_g) \\ \phi_{Btotal} &= \sum_g m_g M_B \Omega_g \left(\frac{\phi_A}{M_A}\right)^{n_g} \left(\frac{\phi_B}{M_B}\right)^{m_g} \exp(\Gamma_g) \end{aligned} \tag{16}$$

The standard chemical potentials μ_g^0 include the appropriate multiples of the standard chemical potentials of the A----A and B----B building blocks and the appropriate multiple of the association energy εkT. For a cyclic group, there is an additional term due to the entropy cost of ring closure, $\Delta S_{loop} = -k\ln G_{cyc}$, where G_{cyc} is the probability density (treated in §2.2 below) for closure of a group g ring:

$$\mu_g^0 = \begin{cases} n_g \mu_A^0 + m_g \mu_B^0 - \varepsilon kT(n_g + m_g) - kT \ln G_{cycl,g} & \text{if cyclic} \\ n_g \mu_A^0 + m_g \mu_B^0 - \varepsilon kT(n_g + m_g - 1) & \text{if linear,} \end{cases} \tag{17}$$

so that Γ_g in the equilibrium and conservation relationships (Equations 15 and 16) is:

$$\Gamma_g = \begin{cases} \varepsilon(n_g + m_i) + (n_i + m_i - 1)\ln(c-1) + \ln G_{cycl,g} & \text{if cyclic} \\ \varepsilon(n_g + m_g - 1) + (n_g + m_g - 1)\ln(c-1) & \text{if linear.} \end{cases} \tag{18}$$

2.2 Entropic Cost of Loop Closure

The entropic cost of loop closure is determined by calculating the probability of loop closure, as follows: For Gaussian linear chains of N Kuhn monomers of length b, the probability density function for the end-to-end vector $\mathbf{r}$ is (*36*):

$$G_{Gaussian}(\mathbf{r}, N) = \left(\frac{3}{2\pi N b^2}\right)^{\frac{3}{2}} \exp\left\{-\frac{3\mathbf{r}^2}{2Nb^2}\right\}. \tag{19}$$

The argument within the exponential $-3\mathbf{r}^2/(2Nb^2) \cong 0$ for $\|\mathbf{r}\| << \langle \mathbf{r}^2 \rangle^{1/2}$, so the probability that the chain ends be within a small distance x of each other, where $x/b \sim O(1)$, is:

$$G_{cyc,Gaussian} = \left(\frac{3}{2\pi Nb^2}\right)^{\frac{3}{2}} \int_0^{2\pi} d\phi \int_0^{\pi} d\theta \sin\theta \int_0^{x/b} dr \cdot r^2 \exp(0)$$
$$= 4\pi \left(\frac{3}{2\pi Nb^2}\right)^{\frac{3}{2}} \int_0^{x/b} dr \cdot r^2 \exp(0) = \left(\frac{6}{\pi N^3}\right)^{\frac{1}{2}} \left(\frac{x}{b}\right)^3 . \tag{20}$$

For real chains, excluded volume interactions of the monomers at chain ends reduce the probability density function $G(\mathbf{r},N)$ by the factor

$$\frac{G_{real}(\mathbf{r},N)}{G_{Gaussian}(\mathbf{r},N)} \sim \left(\frac{\|\mathbf{r}\|}{\sqrt{\langle \mathbf{r}^2 \rangle}}\right)^{\gamma} \qquad \text{for } \frac{\|\mathbf{r}\|}{\sqrt{\langle \mathbf{r}^2 \rangle}} << 1 \tag{21}$$

where the exponent $\gamma \cong 0.28$ (*36*), so that the probability of cyclization becomes

$$G_{cyc,real} \approx 4\pi \left(\frac{3}{2\pi Nb^2}\right)^{\frac{3}{2}} \left(\frac{1}{bN^{\nu}}\right)^{\gamma} \int_0^{x/b} dr \cdot r^{2+g} \exp(0) \sim N^{-3/2-\gamma\nu} \tag{22}$$

where the fractal exponent ν is 0.588 in good solvent. The loop closure probability thus scales as $N^{-3/2}$ for Gaussian chains and $N^{-1.66}$ for swollen chains. The entropic cost of loop closure is simply $\Delta S_{loop} = -k\ln G_{cyc}$.

In dilute or semi-dilute solutions, all chain segments smaller than the thermal blob $g_T \approx b^6/v^2$ (where v is the excluded volume parameter) have Gaussian statistics because excluded volume interactions are weaker than the thermal energy. At the concentrations of interest, the total polymer volume fraction $\phi = \sum_j \phi_j$ is low enough to ignore polymer-polymer overlap, so the following expression is appropriate for the entropic cost of loop closure $\Delta S_{loop} = -k\ln G_{cyc}$ for any cyclic aggregate j:

$$G_{cyc,j} \approx \left(\frac{6}{\pi g_T^3}\right)^{\frac{1}{2}} \left(\frac{x}{b}\right)^3 \left(\frac{M_j}{g_T}\right)^{-1.66} . \tag{23}$$

That is, all chain segments larger than g_T are fully swollen.

2.3 Number of Ways to Form Loops

To determine the number of different loops that can be formed by linking *n* A----A and *n* B----B telechelic chains end-to-end *via* association of A and B end-groups (fig. S3 left), we start by treating telechelics with distinguishable ends (i.e., *n* A_1----A_2 molecules that are indistinguishable from each other, and likewise *n* B_1----B_2 molecules). This maps onto the combinatorial problem of counting necklaces formed using beads of different colors, in which two necklaces are considered equivalent if one can be rotated to give the other. By viewing each supramolecular loop in terms of adjacent pairs of telechelics (with one A_1----A_2 and one B_1----B_2 molecule per pair), they correspond to necklaces made up of *n* "beads" of 4 "colors" (fig. S4). The formula for the number of different necklaces is (*38*):

$$m(n) = \frac{1}{n}\sum_{d|n}\left[\varphi(d)\cdot 4^{n/d}\right]$$

where the sum is over all numbers *d* that divide *n*, and $\varphi(d)$ is the Euler phi function.

In reality, the above formula

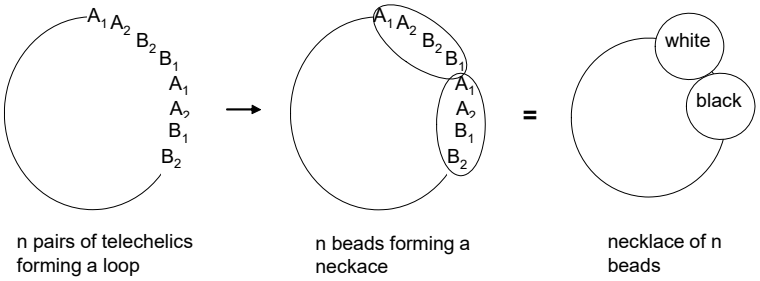

Figure S4 Mapping of polymer loops into necklaces of 4 colors. The 4 colors correspond to: A1A2B1B2, A1A2B2B1, A2A1B1B2, A2A1B2B1. For example, we can choose A1A2B1B2 = black, A1A2B2B1 = white, A2A1B1B2 = blue, and A2A1B2B1 = green.

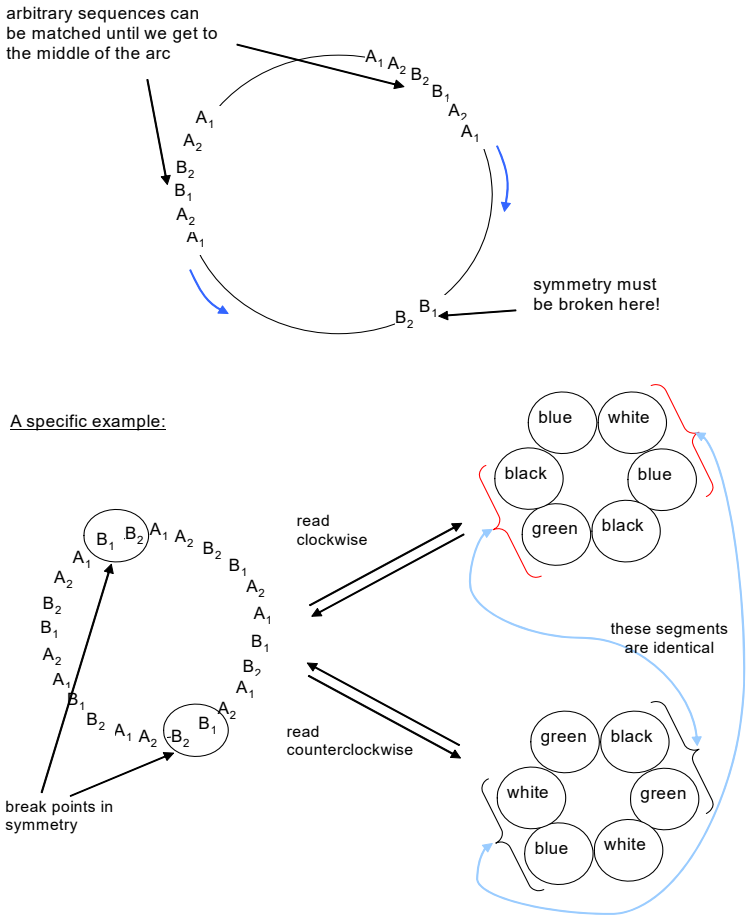

Figure S5 It is not possible to create a loop that "reads" the same clockwise and counterclockwise, so every loop maps into exactly two distinct necklaces. (Color assignments are given in fig. S4).

overcounts the number of ways to form supramolecular loops by a factor of 2. The number of distinct cyclic supramolecules $s(n)$ in the set obtained from n A_1----A_2 and n B_1----B_2 telechelic chains, {loops$_n$}, can be seen to be half the number of distinct necklaces of n beads of four colors {necklaces$_n$} because any supramolecular loop "reads" as a distinct necklace clockwise *vs*. counter-clockwise (fig. S5). While each necklace in {necklaces$_n$} uniquely maps onto a supramolecular loop in {loops$_n$}, every loop in {loops$_n$} maps back to *two* different necklaces, which must belong to {necklaces$_n$}. The elements of {necklaces$_n$} can be arranged pairwise, revealing that there are twice as many elements in {necklaces$_n$} as in {loops$_n$}. Therefore, the number of distinct supramolecular loops $s(n)$ is:

$$s(n) = \frac{1}{2n}\sum_{d|n}\left[\varphi(d)\cdot 4^{n/d}\right] \quad (25)$$

To see that the result obtained by treating the end groups as distinguishable gives the correct result for the actual case in which A-ends are indistinguishable and likewise for B-ends, we consider the reversible association reactions in fig. S6. The reverse reaction rates are all identical. However, the forward reaction for case a (monotelechelic chains) is clearly one-fourth that of case b (telechelics with indistinguishable end-groups). In case c, there are four identical intramolecular scission reactions that give the starting products, so the forward reaction in case c

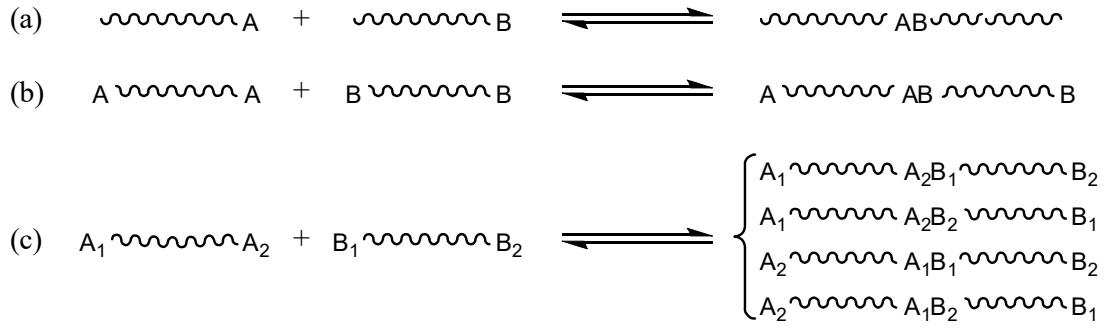

Figure S6 Contact Probabilities and Equilibria

must be 4-fold faster than that of the forward reaction in case a. Thus, the difference in the number of ways to form dimers (Ω_c = 4 compared to Ω_a = 1) can be used to evaluate the increased contact probability of the end-groups to form the product. If the end-groups A, A_1, and A_2 have precisely the same reactivity, and likewise the end-groups B, B_1, and B_2, there cannot be any difference in the equilibrium partitioning of the molecules in cases b and c. We generalize this argument to conclude that the solution to the equilibrium problem presented in fig. S2, where end-groups are indistinguishable, is the solution which we developed for telechelics A_1----

A_2 and B_1----B_2, where end-groups are distinguishable. A less careful modeling of the association of telechelic polymers A----A and B----B might miscalculate the cumulative equilibrium volume fraction of polymer aggregates that fall within any group g by omitting the factor Ω_g in Equation 15.

2.4 Computations

The following procedure was used to calculate the volume fraction of all polymer components (i.e., single-chain starting materials and aggregates of all sizes) at equilibrium, for polymer solutions of A_1----A_2 and B_1----B_2 telechelics of specified molecular weights at specified initial concentrations ϕ_{Atotal} and ϕ_{Btotal}, (polymer components were grouped as shown in fig. S3):

- First, choose a number of groups T_{groups} to include in the analysis (even though there is an infinite number of possible polymer components, we expect that above a certain size, polymer aggregates will have negligible equilibrium volume fraction and can therefore be ignored).
- Calculate n_g, m_g, M_g, Ω_g, $G_{cyc,g}$ (if appropriate), and Γ_g for polymer group g, for $g = 1\ldots T_{groups}$.
- Solve the conservation equations, Equations 16, for (ϕ_A, ϕ_B).
- Calculate ϕ_g for $g = 1\ldots T_{groups}$ using Equation 15.
- Repeat with a new value of T_{groups} twice that of the previous one until changes in the calculated values of ϕ_g from one value of T_{groups} to the next are negligible.

3. CONCLUSIONS

To overcome the problem of chain collapse that occurs when stickers are distributed along a chain, we use a model of ring-chain equilibrium to test the hypothesis that clustering stickers at the ends of polymer chains can be used to generate a sufficient population of mega-supramolecules to exert mist control. We show that linear chains displaying strongly associating, complementary end-groups (A----A and B----B binary mixtures) form linear and cyclic supramolecules that extend to "mega-supramolecules" if the individual building blocks are long enough. Specifically, > 50ppm of mega-supramolecules (ca. 5–10 × 10^6 g/mol) is only achieved with telechelic chains of length > 5 × 10^5 g/mol and a specific range of association

energy, $16 \leq \varepsilon \leq 18$. These theoretical predictions inspired us to develop synthetic routes to the predicted molecules,

Experimentally, we chose poly(1,5-cyclooctadiene) as the polymer backbone, which corresponds to a 1,4-polybutadiene with 75% cis, 25% trans and 0% short side branches. Thus, we conclude that the required chain length for PCOD should be similar to that predicted with parameters based on PI and PB as discussed in §1.2. Unlike the model, real polymers are polydisperse. The telechelics synthesized using ROMP/CTA have $M_w/M_n = 1.5 \pm 0.1$, so we apply the guidance from theory by targeting polymers in range from $M_w = 5 \times 10^5$ g/mol to $M_n = 5 \times 10^5$ g/mol ($M_w = 10 \times 10^5$ g/mol). The remarkable polymers described in the paper demonstrate the success of our theoretical model and our parameter estimation using prior literature on 1,4-PI and 1,4-PB.

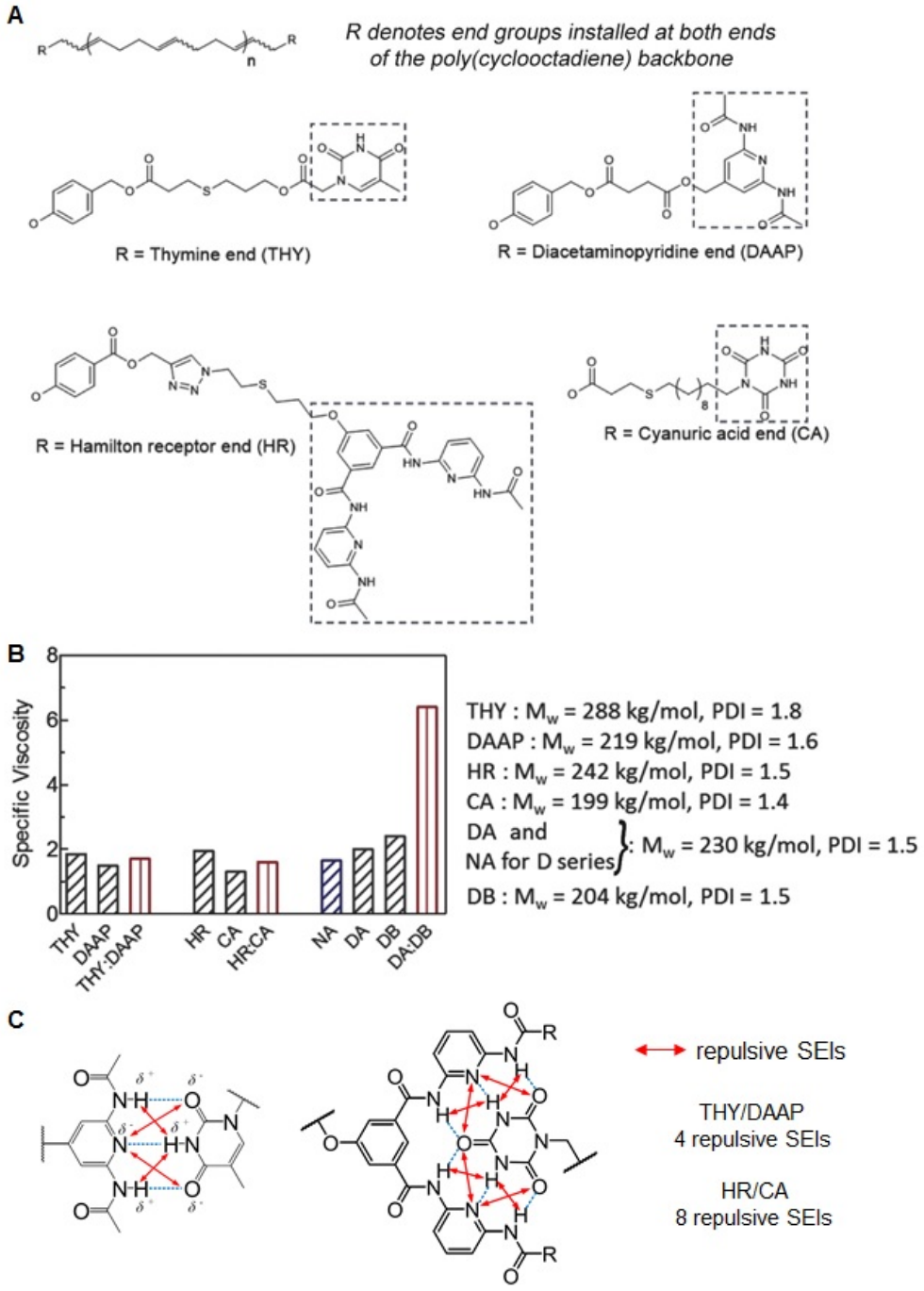

Figure S7

Selection of the end-groups. (A) Chemical structures and molar masses of the end-associative polymers (excepting isophthalic acid/tertiary amine functionalized ones that are shown in Fig. 1). **(B)** Specific viscosities of telechelic polymers at 8.7 mg/ml total polymer in 1-chlorododecane. Based on the literature on complementary polyvalent hydrogen-bonding pairs, we were surprised that a 1:1 THY/DAAP solution had a viscosity equal to the average of the viscosities of the individual components' solutions. We were even more surprised when the 1:1 HR/CA showed a viscosity equal to the average of the individual components. Only the DA/DB pair shows enhancement in viscosity relative to the individual telechelic polymers. **(C)** Illustration of secondary electrostatic interactions (SEIs) in THY/DAAP and HR/CA pair.

Our data suggest that, despite the simplicity of carboxylic acid and tertiary amine structures, the DA/DB pair provides stronger end-association than the hexadentate HR/CA pair. We attribute this difference primarily to the 3- to 4-fold greater strength of charge-assisted hydrogen bonds (as is the case of DA/DB) relative to ordinary hydrogen bonds (in both THY/DAAP and HR/CA). Therefore, in non-polar solvent the sum of the two charge-assisted hydrogen-bonds in a DA/DB pair is likely stronger than the sum of the six ordinary hydrogen bonds in the HR/CA pair. In addition, the DA/DB pair does not suffer from the adverse effect of repulsive secondary electrostatic interactions (SEIs) that occur when the both partners have H-bond donors and H-bond acceptors: in the HR/CA pair, the polarities of the six hydrogen-bonds alternate in direction, thus decreasing the overall strength of HR/CA association. We estimate for THY/DAAP (association constant in deuterated chloroform at 25°C = 10^3 M^{-1}) (*39*), three primary hydrogen bonds contribute -24 kJ/mol and four repulsive SEIs contribute +12 kJ/mol (net *ca*. 5*kT*); and for HR/CA, six hydrogen bonds contribute -47 kJ/mol and eight repulsive SEIs contribute +23 kJ/mol (net *ca*. 10*kT*, part **C**). The literature value of the association constant for a polymer-bound HR/CA pair in deuterated chloroform at 25°C is 1.5×10^4 M^{-1} (*7*), corresponding to an end-association strength of 9.6 *k*T, in good agreement with our value of 10 *k*T estimated from SEI analysis. As described in the main body text, the strength of the DA/DB pair is estimated to be 16-18 *k*T. The difference in estimated strength between DA/DB and HR/CA is consistent with our experimental results in (**B)**. Together, SEI analysis and shear viscometry reveal that HR/CA does not, in fact, have an association constant in non-polar solvents that is high enough to drive long telechelic polymers to form mega-supramolecules at concentrations of interest in the scope of the present work.

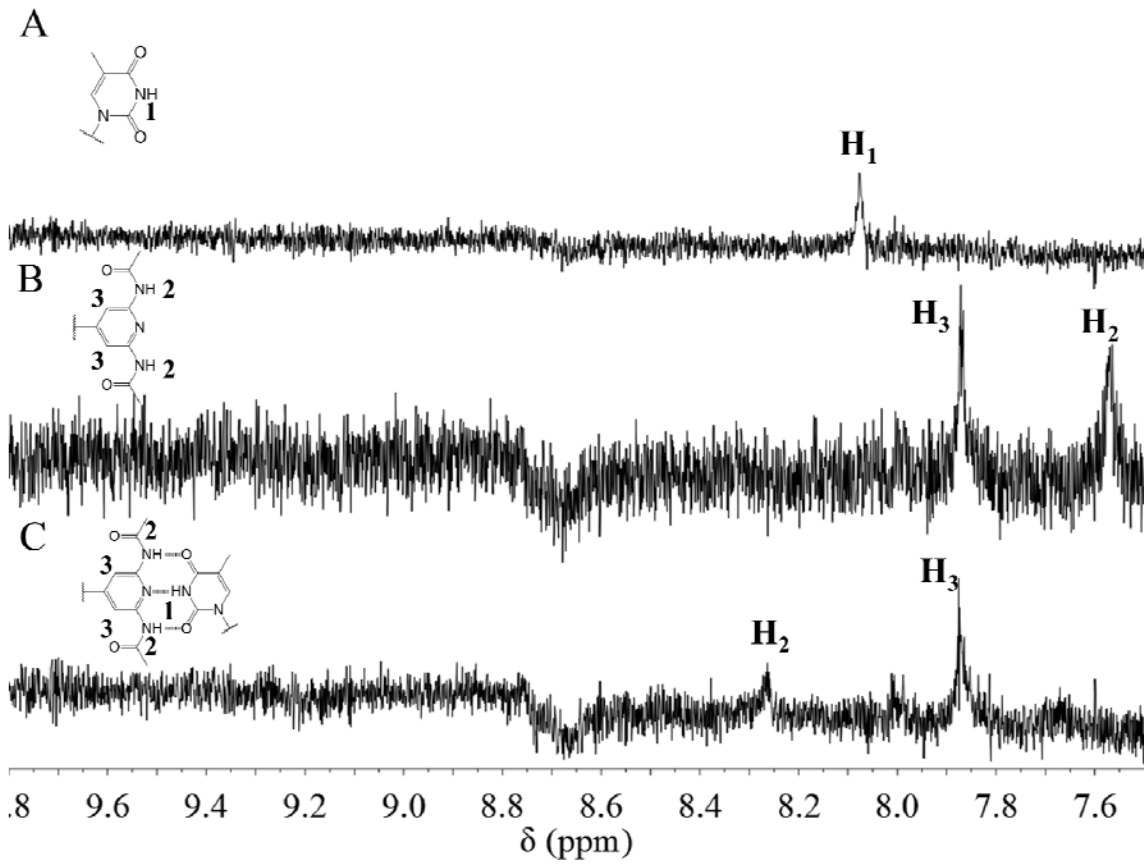

Figure S8

Expanded ^{1}H NMR (500 MHz) spectra of telechelic polymers in $CDCl_3$ (ρ=1.5g/ml) at 15mg/ml. **(A)** PCOD of M_w = 288 kg/mol with THY end groups give a weak signal because they are only present at 160μM, **(B)** PCOD of M_w = 219 kg/mol with DAAP end groups give a weak signal because they are only present at 200μM, and **(C)** a mixture of the two polymers with a mass ratio of 1:2, determined by titration to be sufficient to reach the asymptotic chemical shift of H_1, in accord with prior literature (*39*). The concentration of polymer in solution is approximately 1%wt total (i.e., 5mg/ml of 288k THY; and 10mg/ml of 219k DAAP). The peak for H_2 is shifted downfield in the mixture (the peak for H_1 is expected to be shifted to approximately 9.5ppm, but it is not observed, consistent with literature reports of greater broadening of H_1 than H_2). These changes in ^{1}H NMR spectra are in qualitative agreement with previous literature, which describes relatively small molecule building blocks (<10kg/mol) for supramolecular assembly (*39*).

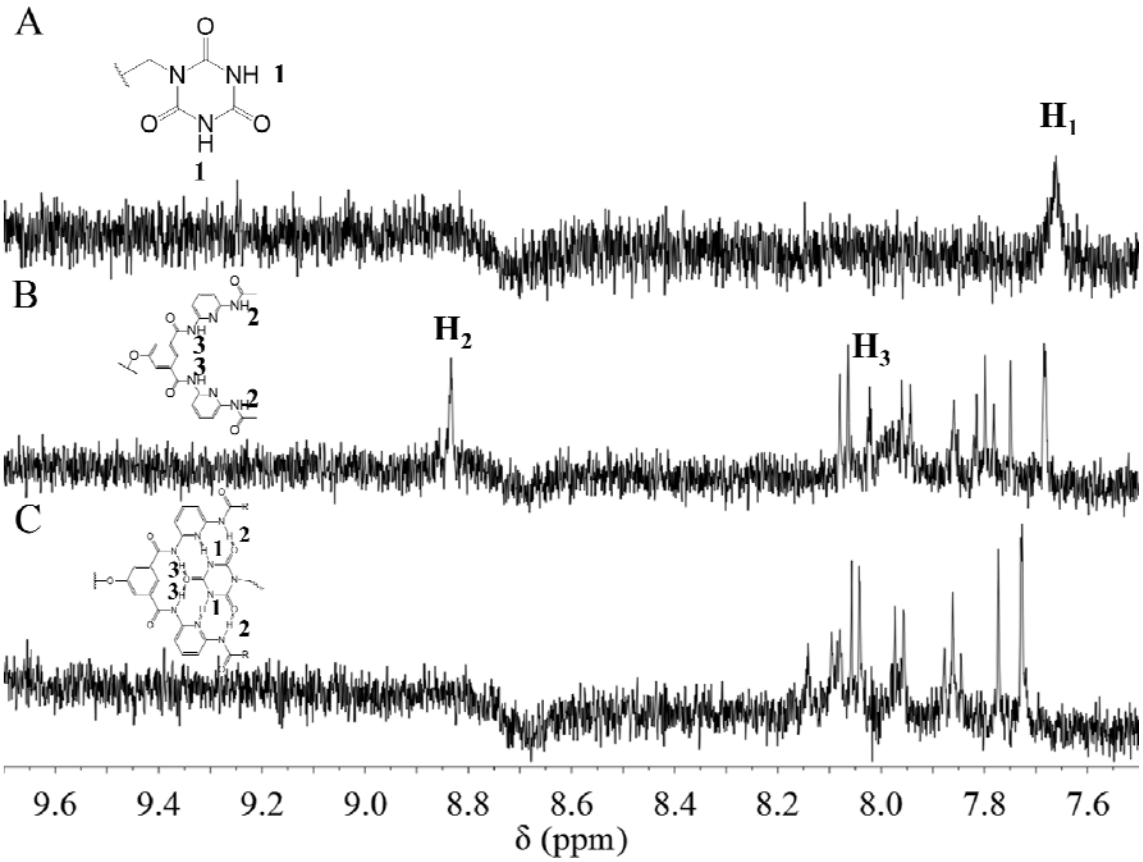

Figure S9

Expanded ^{1}H NMR (500 MHz) spectra of $CDCl_3$ solutions of telechelic polymers in $CDCl_3$ (ρ=1.5g/ml) at 15 mg/ml. (A) PCOD of M_w = 200 kg/mol with CA end groups give a weak signal because they are only present at 225μM. **(B)** PCOD of M_w = 240 kg/mol with HR end groups give a weak signal because they are only present at 188μM, and **(C)** a mixture of the two polymers with a mass ratio of 1:2, sufficient to reach the asymptotic chemical shift of H_1, in accord with prior literature (*7*). The concentration of polymer in solution is approximate 1%wt total (i.e., 5mg/ml of 200k CA; and 10mg/ml of 240k HR). Both peaks for H1 and H_2 are shifted downfield in the mixture (the peak for H_1 is expected to be shifted to approximately 12.5ppm and that for H_2 to 9.7ppm, but they are not observed, consistent with literature reports of broadening of H_1 and H_2). These changes in ^{1}H NMR spectra are in qualitative agreement with previous literature, which describes relatively small molecule building blocks (<10kg/mol) for supramolecular assembly (*7*).

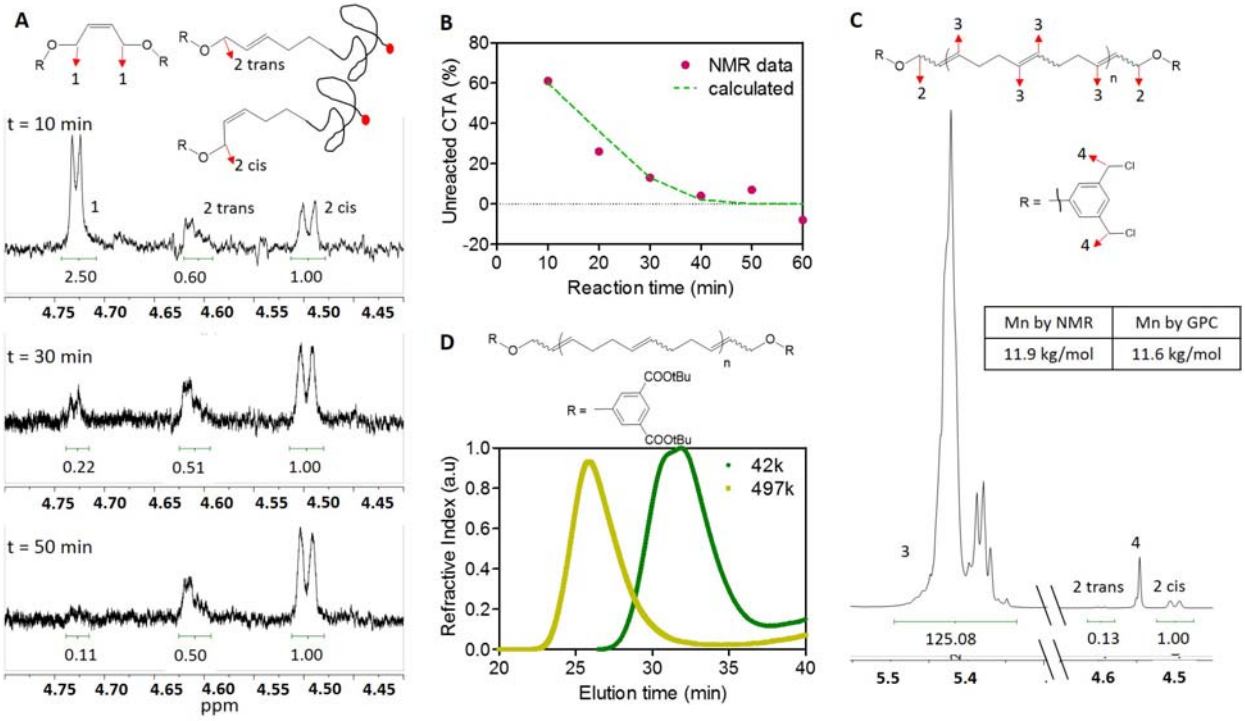

Figure S10

Incorporation of CTA into polymer during the first stage of two-stage ROMP of COD, and chain extension to long telechelics in the second stage. (A) ^{1}H NMR of characteristic peaks for di(di-*tert*-butyl-isophthalate) CTA (structure of end-group shown in fig. S12), unreacted CTA (proton 1) and CTA incorporated into macromer (proton 2), at three time points; the integrations of the peaks were used to calculate the percentage of unreacted CTA, shown in part **B**. **(B)** Kinetic curves show that the peaks characteristic of the unincorporated CTA are already difficult to quantify in the sample taken after 40min, and it is not evident for the sample taken at 1 hour (given the magnitude of the noise in the spectra, the amount of unincorporated CTA is less than 3%). Dashed curve is calculated based the data point at 10 min assuming exponential decay of unreacted CTA. **(C)** In an example with di-chloro PCOD, the M_n calculated by NMR is in good agreement with that measured by GPC, considering the inherent uncertainty in NMR integration and the inherent uncertainty in GPC measurement (5-10%). **(D),** GPC traces show no indication of macro CTA (42 kg/mol) in the chain-extended telechelics (structure shown in **D**, 497 kg/mol) produced in the second step.

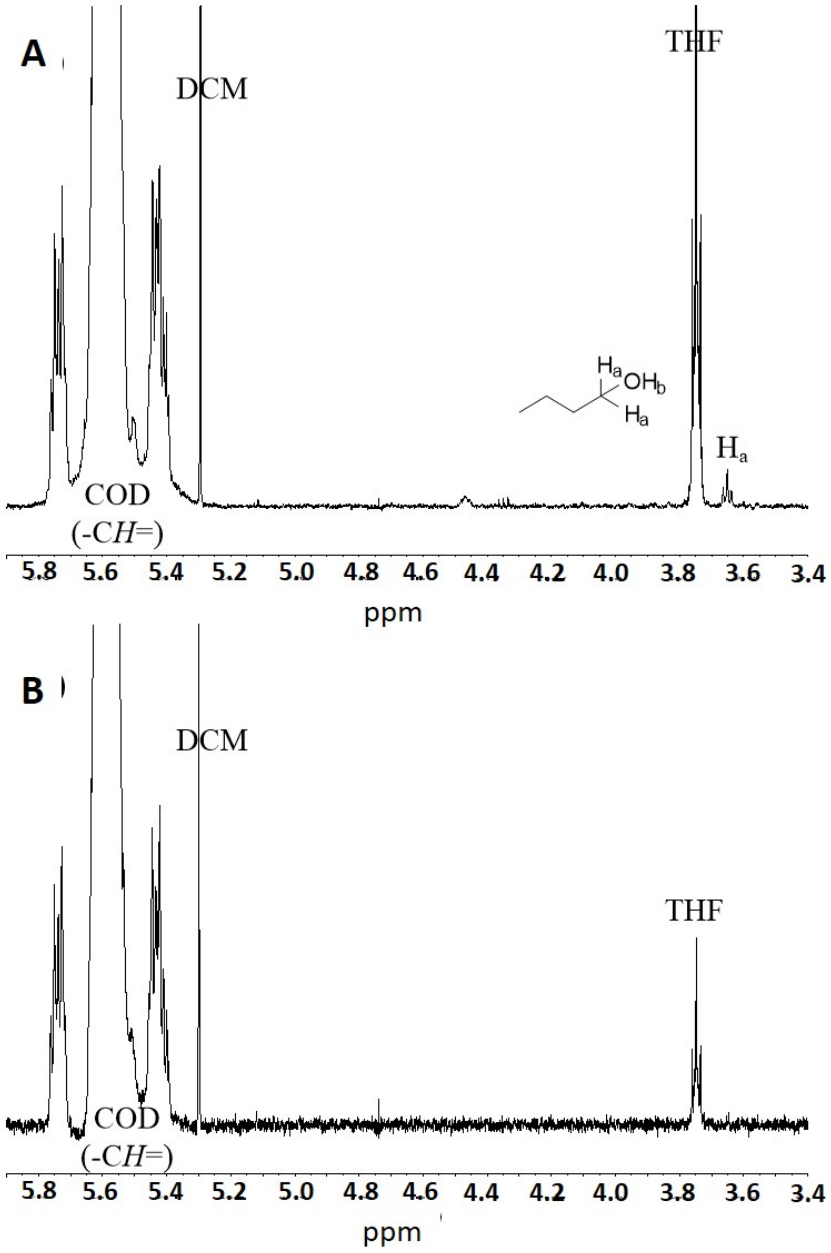

Figure S11
^{1}H NMR spectra of increasingly purified COD in the range from 3.4 to 5.9ppm. (A) COD after BH_3·THF treatment and vacuum distillation (containing ~330 ppm of butanol based on integration). (**B)** COD further purified with magnesium silicate/CaH_2 treatments (to show removal of butanol and the resulting purity of COD used as monomer).

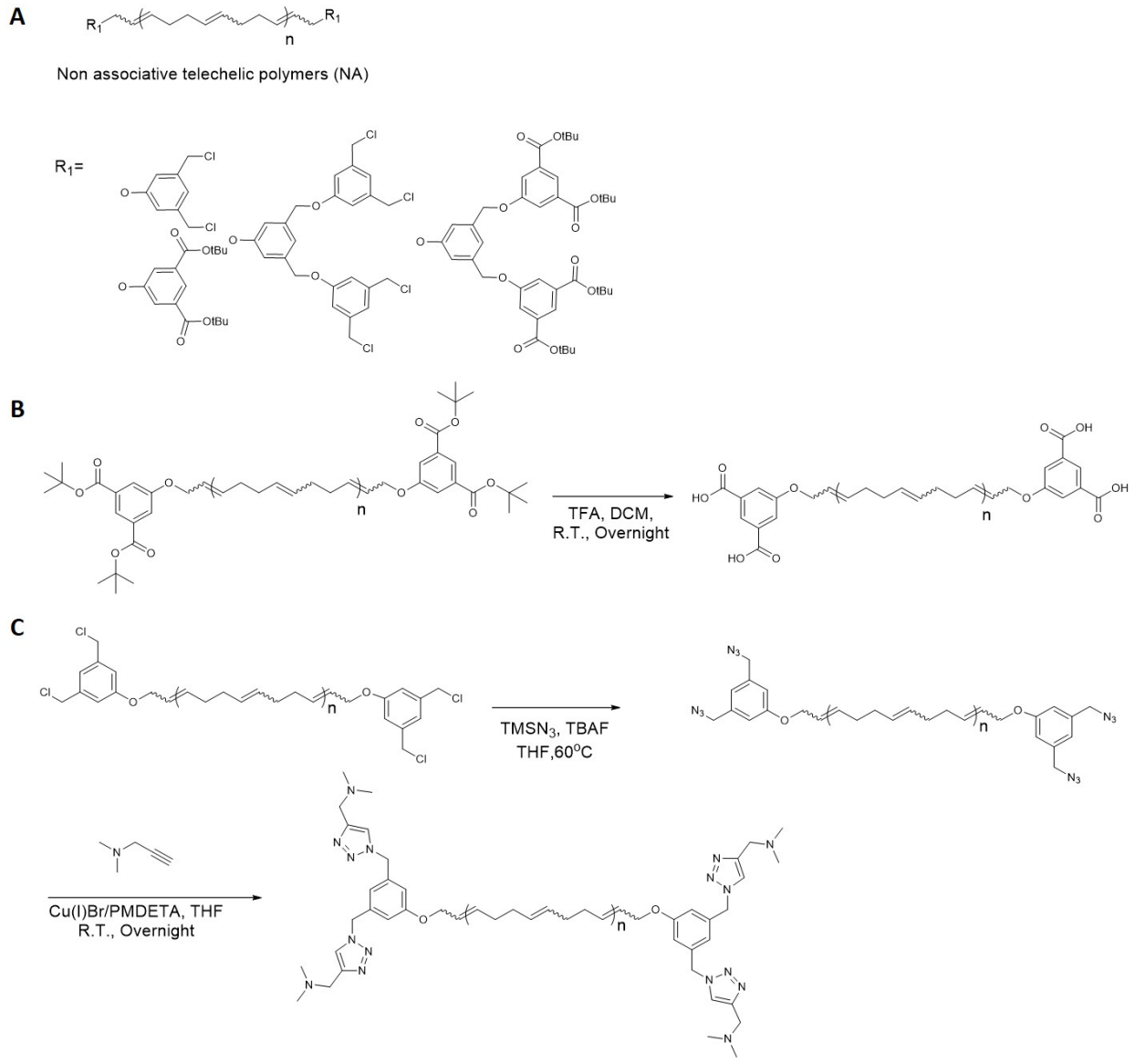

Figure S12
(A) Structures of non-associative (NA) end-groups and the conversion from NA to associative end-groups: (B) isophthalic acid and (C) tertiary amine (products shown in Fig. 1). Isophthalic acid end groups are obtained by deprotection of the tBu groups in the tBu-ester-ended non-associative precursor. Tertiary amine end-groups are obtained via conversion of chloride end-groups to azide end-groups, followed by an alkyne/azide cycloaddition.

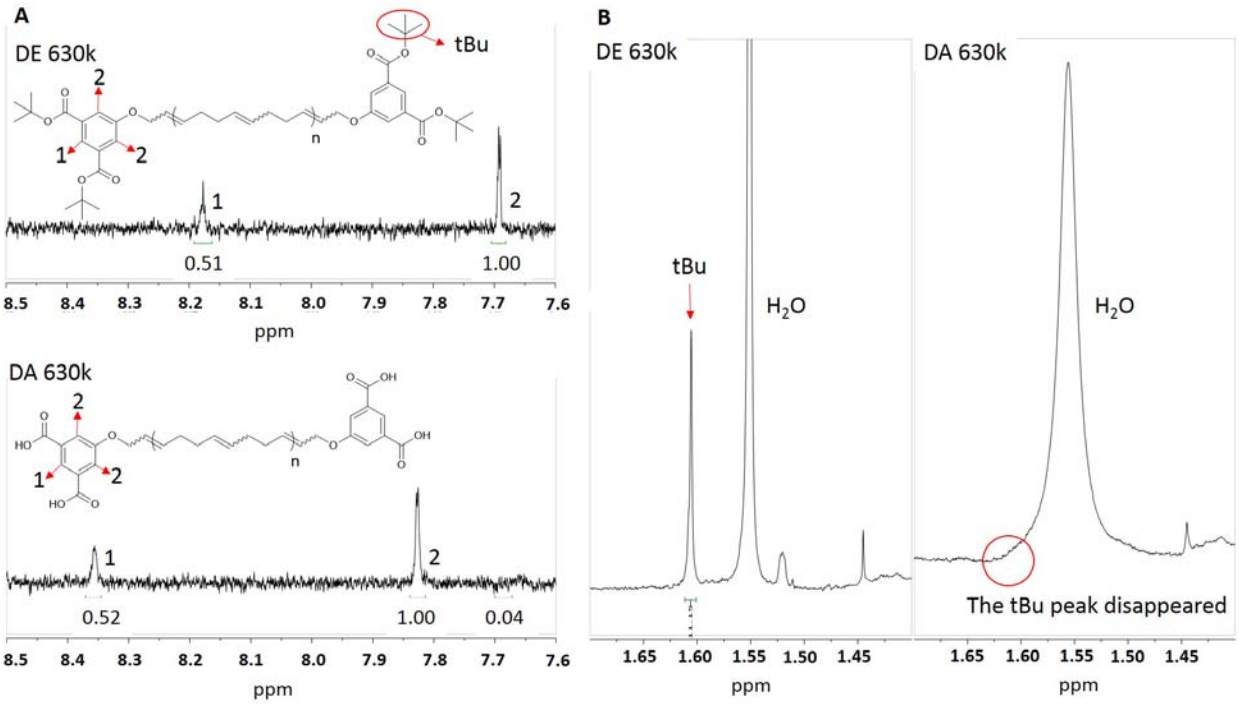

Figure S13
^{1}H NMR spectra of tBu-ester ended (DE) and isophthalic acid ended (DA) polycyclooctadiene (M_w = 630 kg/mol) to show high degree of conversion of the end-groups. **(A)** the peaks for protons on the phenyl ring (protons 1 and 2) shift due to the removal of tBu. Comparing the integration of peak for proton 2 (~7.82ppm) with that of the baseline at ~ 7.7 ppm (where the peak for proton 2 in DE is, see **A** top) in the spectrum of DA (**A** bottom) shows a < 5% (1 comparing to 0.04) potential unconverted end-groups due to baseline noise. **(B)** the peak for tBu group disappears in the spectrum for DA, indicating removal of the tBu group.

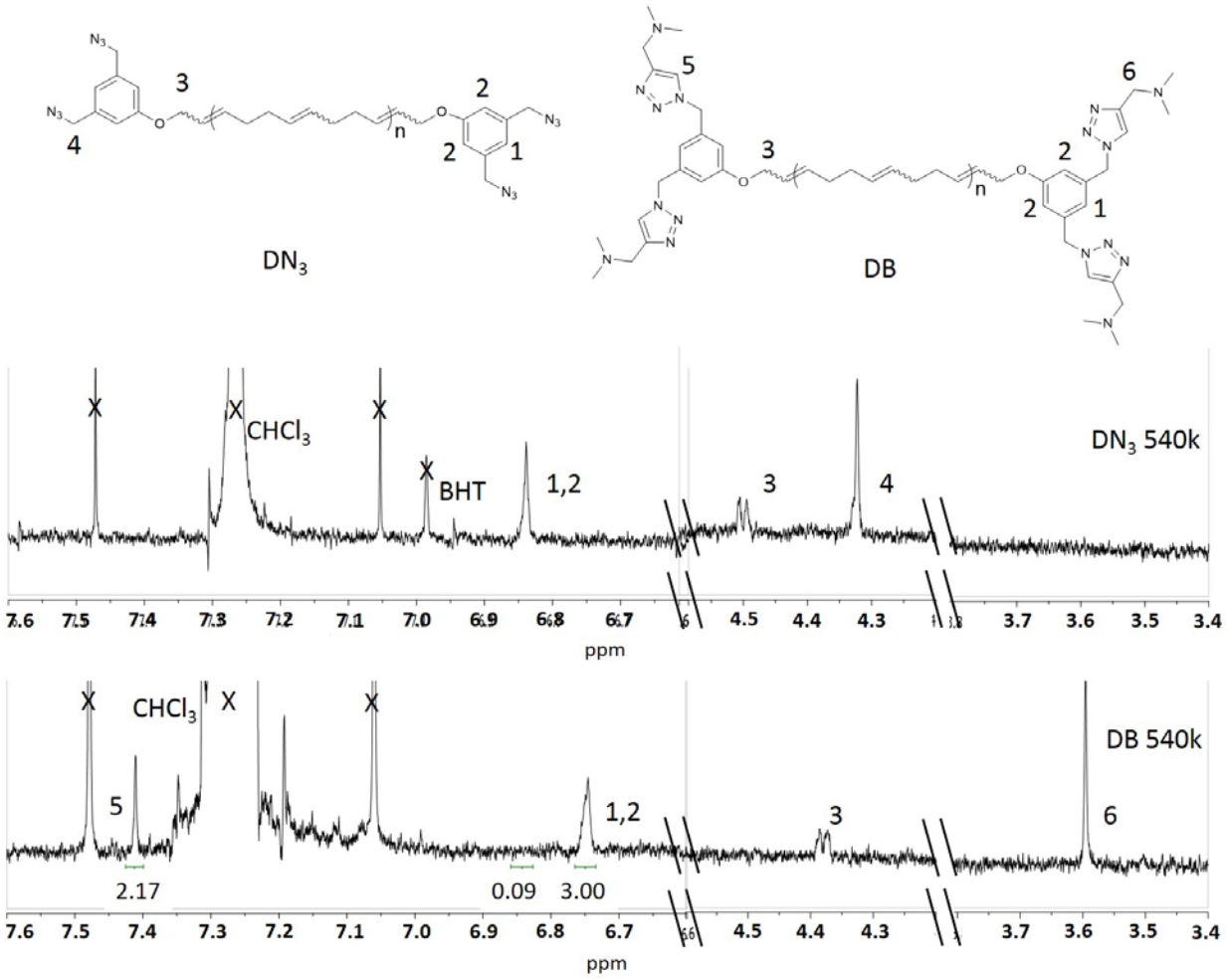

Figure S14
^{1}H NMR spectra of azide ended (DN_3) and tertiary amine ended (DB) polycyclooctadiene (M_w = 540 kg/mol) to show high degree of conversion of the end-groups. In the spectrum for DB (bottom), the presence of a peak at 7.4 ppm indicates the formation of triazole rings (proton 5), absent in DN_3's spectrum (top). The peak for protons on the phenyl ring (at positions 1 and 2) shifts from 6.85ppm before (top) to 6.75ppm after the cycloaddition reaction (bottom): integration of the peak for protons at 1 and 2 (~6.75 ppm, relative integral integral = 3) in the spectrum of DB (bottom) and of the baseline at ~ 6.85 ppm (no detectable 1,2 of DN_3, relative integral = 0.09) places an upper bound of < 5% unconverted end-groups.

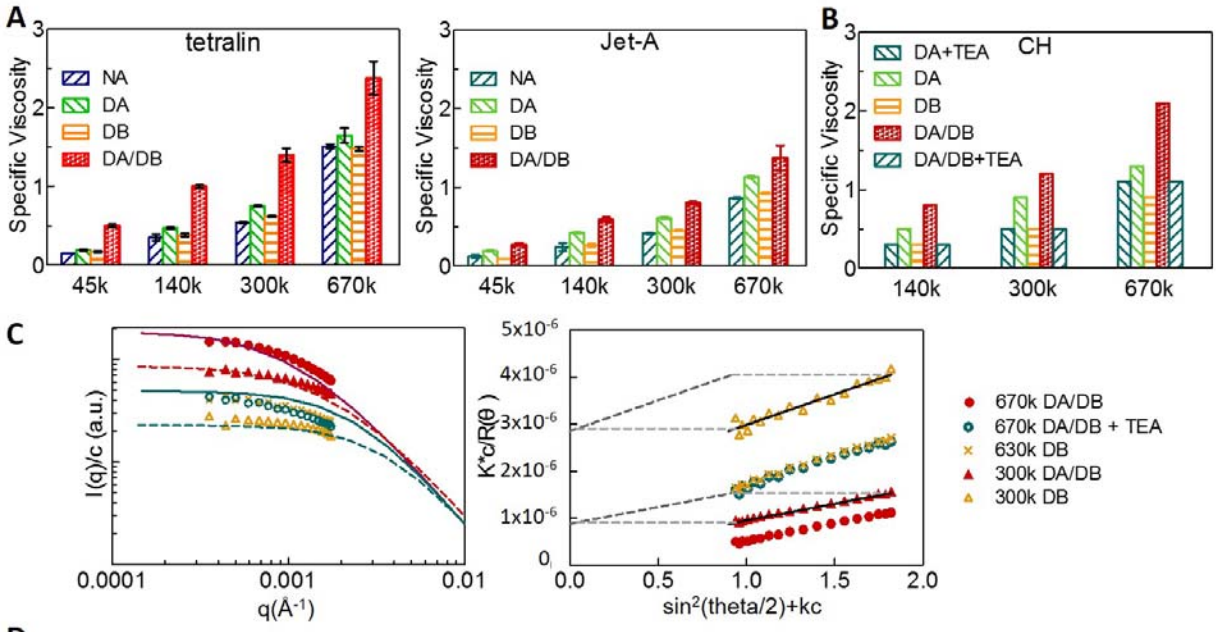

D

		Associated	Not associated	
			DA/DB+TEA	DB
670k DA/DB	app *Mw*	(2.2 ± 0.2) e+6 g/mol	(6.3 ± 0.5) e+5 g/mol	(6.1 ± 0.5) e+5 g/mol
	app Rg	87 ± 4 nm	58 ± 3 nm	58 ± 3 nm
300k DA/DB	app *Mw*	(1.1 ± 0.4) e+6 g/mol	-	(3.2 ± 0.3) e+5 g/mol
	app Rg	60 ± 3 nm	-	36 ± 6 nm

Figure S15

Formation of supramolecules in equimolar solutions of α,ω-di(isophthalic acid) polycyclooctadiene, α,ω-di(di(tertiary amine)) polycyclooctadiene (DA/DB), with non-associated controls (NA, see fig. S9 top; and solutions treated with an excess of a small-molecule tertiary amine, triethylamine, TEA at 10 µl/ml). **(A)** Effect of chain length (k refers to kg/mol) on specific viscosity of telechelics in tetralin and Jet-A (2 mg/ml) at 25°C. **(B)** Effect of TEA (2.5 µl/ml) on the viscosities of associative telechelic polymers DA/DB. **(C)** Left: Static light scattering shows that association between DA and DB chains (circle: 670k series; triangle: 300k series) in CH at 0.22mg/ml (0.028%) produces supramolecules (filled), which separate into individual building blocks (x) when an excess of a small-molecule tertiary amine is added (open symbols, 10 µl/ml of triethylamine, TEA). Curves show predictions of the model, details below. Right: Zimm plot of the same static light scattering data shown in Left part. Lines indicate the fitting to the Zimm equation and dashed lines indicate the extrapolation that was used to evaluate the intercept at zero concentration, zero angle; the slope of the line and the value of the intercept are used to evaluate the apparent M_w and apparent R_g, details below. **(D)** Resulting values of apparent M_w and R_g for the five polymer solutions in part **C**.

- The effect of chain length on specific viscosity of telechelics in tetralin and Jet-A (**A**) is similar to that in cyclohexane (Fig. 2A). The specific viscosity of telechelics in Jet-A is generally lower than that in tetralin or cyclohexane. This effect is observed even for the non-associative polymers (NA), indicating that the backbone adopts a more compact conformation in Jet-A. It would be difficult to predict this effect a priori, because Jet-A is a mixture of many hydrocarbons with number of carbon atoms between 6 and 16, including some components that are good solvents for PCOD and some that are theta solvents for PCOD.

- The model calculations (**C**) show the effect of doubling the backbone length for complementary telechelics with association energy 16kT, backbone lengths corresponding to a PCOD of 1,000 kg/mol (red) or 500 kg/mol (blue) at 1,400 ppm concentration in a good solvent on the scattering pattern computed from the distribution of supramolecules (solid, supramolecules up to 9 telechelics; dashed, corresponding perfectly monodisperse non-associative telechelics). To compare with the experimental data, we allowed a single vertical shift to be applied to all four curves and a single horizontal shift. The distributions of supramolecules are shown in fig. S16.
- The Zimm fitting was performed using Wyatt Astra Software (version 5.3.4): illustrations for the 300k DA/DB and 300k DB are shown, with the linear regression through the data (black solid line) extrapolated to zero-concentration (horizontal light gray dashed line) and to zero angle (oblique gray dashed line). The y-intercept of the zero-angle zero-concentration extrapolation gives the apparent $M_{w,}$ while its slope is used to compute the apparent R_g.

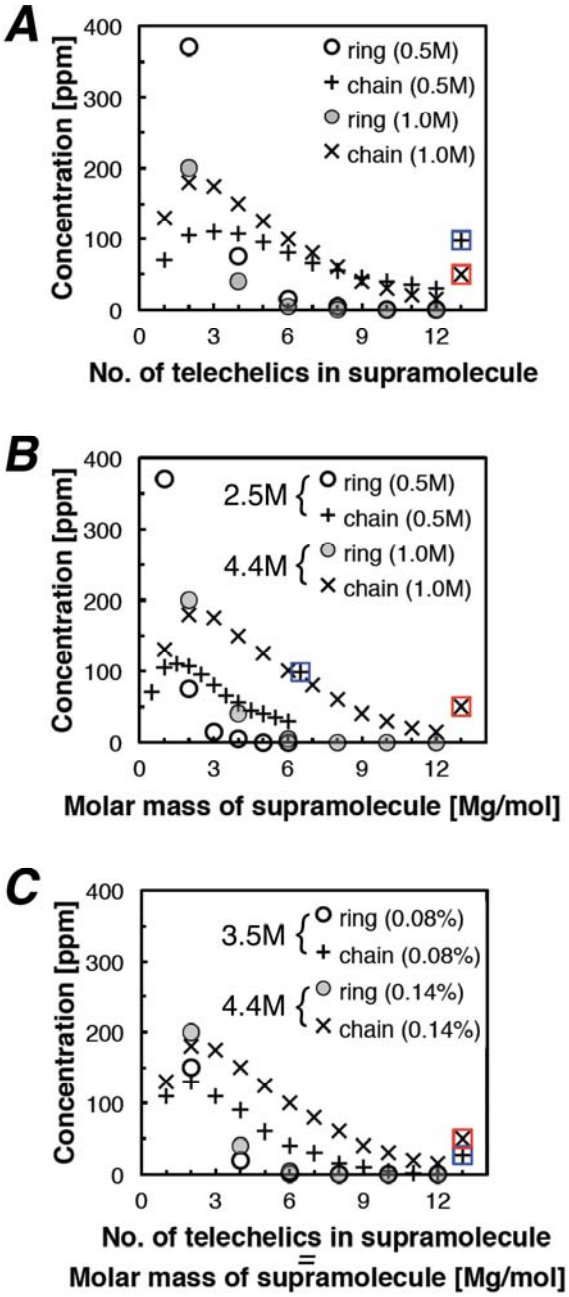

Figure S16

Interplay of telechelic length and concentration in a stoichiometric mixture of complementary end-associative telechelics in the regime of long telechelics (corresponding to ≥0.5Mg/mol for high-1,4-polyisoprene, high-1,4-polybutadiene or polycyclooctadiene) and low concentration (≤0.14% wt/wt), facilitating comparison among the three different cases (fig. S1, center column), in terms of both the number of telechelics in each supramolecular species and the molecular weight of each supramolecular species. Symmetric cases are considered (donor and acceptor telechelics have the same length). End association energy between donor and acceptor end-groups is 16*kT*. The concentration of each distinct species is shown for supramolecules composed of up to 12 telechelics; the symbol in a square outline represents the sum of all supramolecules containing 13 or more telechelics (red square around x is for the case 1.0Mg/mol chains at 1,400ppm concentration; the blue square around + is for the other case in each graph).

(A) Effect of telechelic length on the distribution of the number of telechelics in a supramolecule, given as the concentration in ppm wt/wt of each species, cyclic (circles) or linear (x or +), at a fixed total concentration of 1400ppm. **(B)** The same distributions as in A, presented in terms of the molar mass of the supramolecules; the weight-average molar mass of the supramolecules is given to the left of the legend. **(C)** Effect of concentration on the distribution of supramolecules for telechelics of 1M g/mol (hence, the number of telechelics in a given supramolecule is also its molar mass in Mg/mol) Note the results for the 1Mg/mol telechelics at 0.14% concentration is given in all three graphs to facilitate comparisons.
In the regime of long telecheclics at low concentration, the equilibrium distribution of rings is dominated by rings composed of 2 telechelics (one donor + one acceptor) or 4 telechelics (in a donor/acceptor system, rings can only close if the number of telechelics is even). The fraction of telechlics "lost" to these rings is cut in half by doubling the length of the telechelics from 0.5M to 1.0Mg/mol, increasing the formation of linear supramolecules (**A**). Increasing the length of the backbone also increases the size of the supramolecules at each number of telechelics per supramolecules (compare **B** to **A**); consequently, increasing the telechelic length strongly increases the population of "mega-supramolecules" (the sum of the concentrations of all species having molecular weight greater than 5Mg/mol increases from 200ppm for 0.5Mg/mol telechelics to 400ppm for 1.0Mg/mol). Dilution, here from 1,400ppm to 800ppm wt/wt, favors the formation of "small" supramolecules composed of 4 or fewer telechelics at the expense of mega-supramolecules (here, the sum of all species >5Mg/mol falls from 400ppm to 230ppm). Note that "small" species assembled from 3-4 telechelics were already the dominant ones at higher concentration, so dilution has relatively mild effects on the weight average molecular weight (numbers shown to the left of the legend in **C**). For further details on the model, please see modeling.

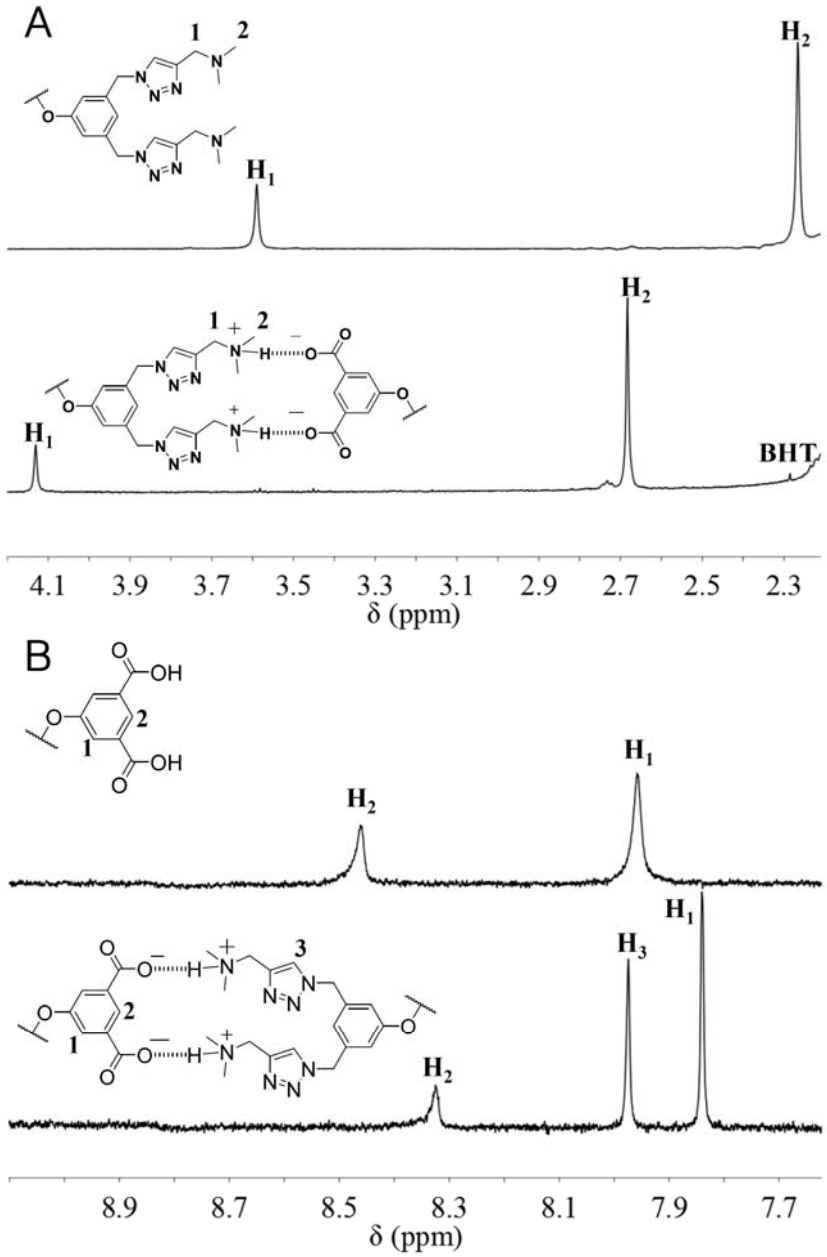

Figure S17

^{1}H NMR spectra of isophthalic acid ended (DA) and di(tertiary amine) ended (DB) polycyclooctadienes (M_w = 45 kg/mol) and 1:1 molar mixture of DA/DB in deuterated chloroform ($CDCl_3$) show that carboxylic acid – amine hydrogen bonds dominate over carboxylic acid – carboxylic acid hydrogen bonds. **(A)** ^{1}H NMR peaks due to hydrogens on carbons adjacent to nitrogens of tertiary amine groups of DB (methylene protons **1**; methyl protons **2**) shift downfield when they form charge-assisted hydrogen bonds with carboxylic acid groups of DA (cf. upper to lower spectra: **1** shifts from 3.59 to 4.13ppm; and **2** shifts from 2.27 to 2.68ppm). **(B)** ^{1}H NMR peaks due to hydrogens on the phenyl ring of DA shift upfield upon formation of charge-assisted hydrogen bonds between carboxylic acids and tertiary amines (cf. upper to lower spectra: **1** shifts from 7.96 to 7.84ppm; and **2** shifts from 8.46 to 8.32ppm). In the present case, the hydrogen of the carboxylic acid itself is not observable due to extreme broadening resulting from rapid exchange with trace H_2O in the solvent. The formation of acid-

amine charge-assisted hydrogen bonds entirely consumes the available tertiary amine (**A**, lower spectrum, no detectable peak at 3.59ppm indicates less than 3% of non-associated amine) and eliminates acid-acid hydrogen bonds (**B**, lower spectrum, no detectable peak at 8.46ppm indicates less than 3% of acid-acid association). The absence of acid-acid pairing is consistent with literature values of the association constants for carboxylic acid self-association (400 M^{-1}) and for charge assisted-hydrogen bonds that form between tertiary amine and carboxylic acid in chloroform (5×10^4 M^{-1}, *40*).

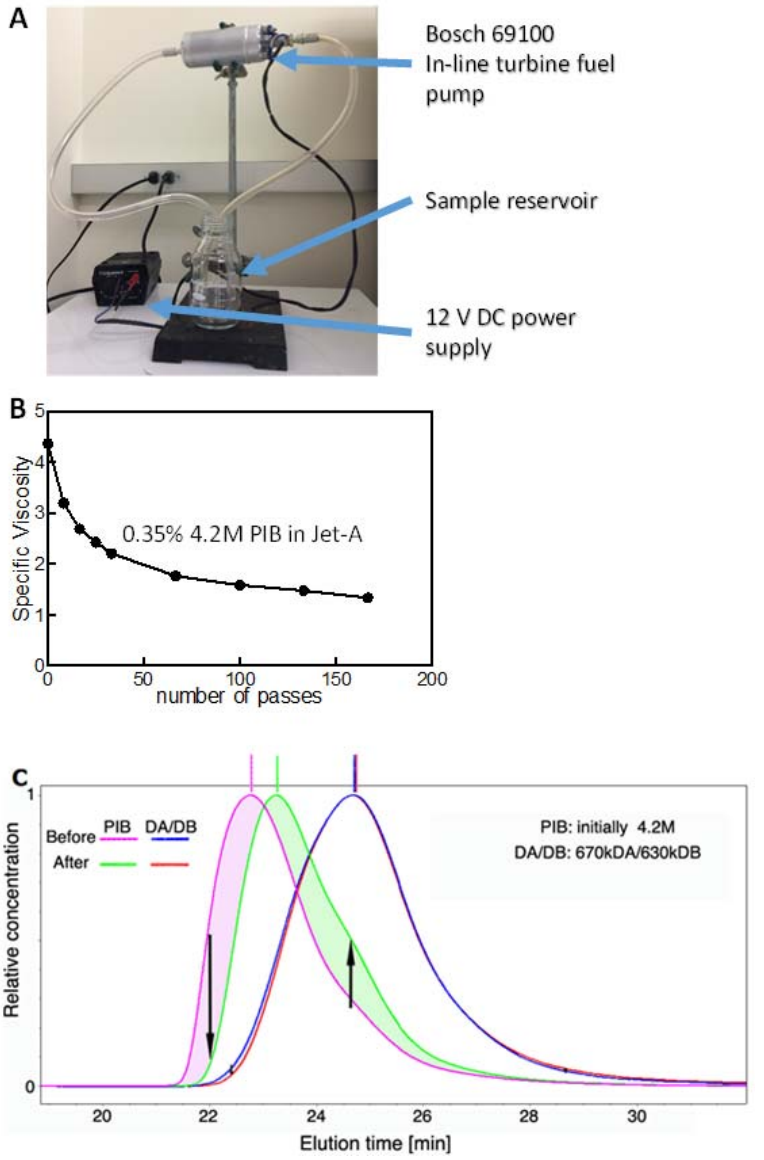

Figure S18

(A) Home-built apparatus for "shear degradation" test. Ultra-long covalent polymers undergo chain scission in intense flows, such as turbulent pipeline flow and, especially, passage through pumps. This phenomenon is called "shear degradation." To subject polymer solutions to conditions that approach the asymptotic limit of shear degradation (i.e., the backbone length is reduced to the point that further chain scission is very slow), we recirculated a relatively small volume of sample (50ml) through a turbine fuel pump at room temperature for 60 s (approximately 60 passes through the pump using a flow rate of 3 L/min) using a Bosch 69100 In-line Electric Fuel Pump at 12 V. To prevent cross-contamination, the pump was rinsed 4 times with approximately 200 mL of hexanes, followed by drying under reduced pressure at 40°C overnight. After recirculation, 'sheared' samples were collected in 100 mL glass jars and stored at -30°C. **(B)** An initially 4,200 kg/mol PIB at a concentration of 0.35% in Jet-A shows the decrease in specific viscosity indicative of shear degradation with increasing number of passes through the pump. Notice that over 80% of the asymptotic degradation is induced by approximately 60 passes, leading to the selection of the conditions described above. **(C)** GPC

validation of "shear degradation" test using PIB and confirmation that associative polymers resist degradation. Polyisobutylene having an initial M_w = 4,200 kg/mol (Before) is dissolved in Jet-A at a concentration of 0.35%wt and recirculated through the fuel pump as described in (A) for 60s (approximately 50 passages through the pump) and the resulting solution analyzed by GPC (After). The shift to lower molecular weight (M_w = 2,300 kg/mol) confirms that the recirculation treatment does indeed induce shear degradation in accord with the literature on multi-million molecular weight polymers in dilute solution. The shaded area on the left (pink) shows the population of chains that were degraded and, in accord with literature, the right shaded area (green) shows the population of chains that was produced from scission of longer PIB chains, which accords with chains breaking preferentially near the midpoint of their backbone. The length at which the before and after traces cross is the chain length for which the rate of degradation matched the rate of production (due to scission of much longer chains).
A stoichiometric solution of telechelic polycyclooctadienes bearing either isophthalic acid groups at each end (DA, initial M_w = 670k g/mol) or two tertiary amine groups at each end (DB, initial M_w = 630k g/mol) in Jet-A at concentration of 0.3%wt was also analyzed by GPC in as-prepared form (Before; detected M_w = 747 kg/mol)) and after 60s recirculation in apparatus (After; detected M_w = 718 kg/mol). A small decrease in the population of the longest chains (fastest elution time; $M_w \geq$ 1,200 kg/mol) may occur (see the area shaded in pale blue with a small downward pointing arrow). We consider this insignificant as it is near the detection limit of the instrument; relative to the GPC trace of the as prepared DA/DB solution, the GPC trace "after" the recirculation treatment may also show a minute increase in the population of chains on the right side of the peak (shaded pink and marked with a small upward arrow). The latter change is too small for us to confidently measure with our GPC instrument. Note that the possible degradation of the DA and DB telechelics occurs only where the individual polymers are so long that they would be vulnerable to shear degradation. Thus, "stress relief" by reversible dissociation appears to protect all telechelics < 1,200 kg/mol from hydrodynamic chain scission.

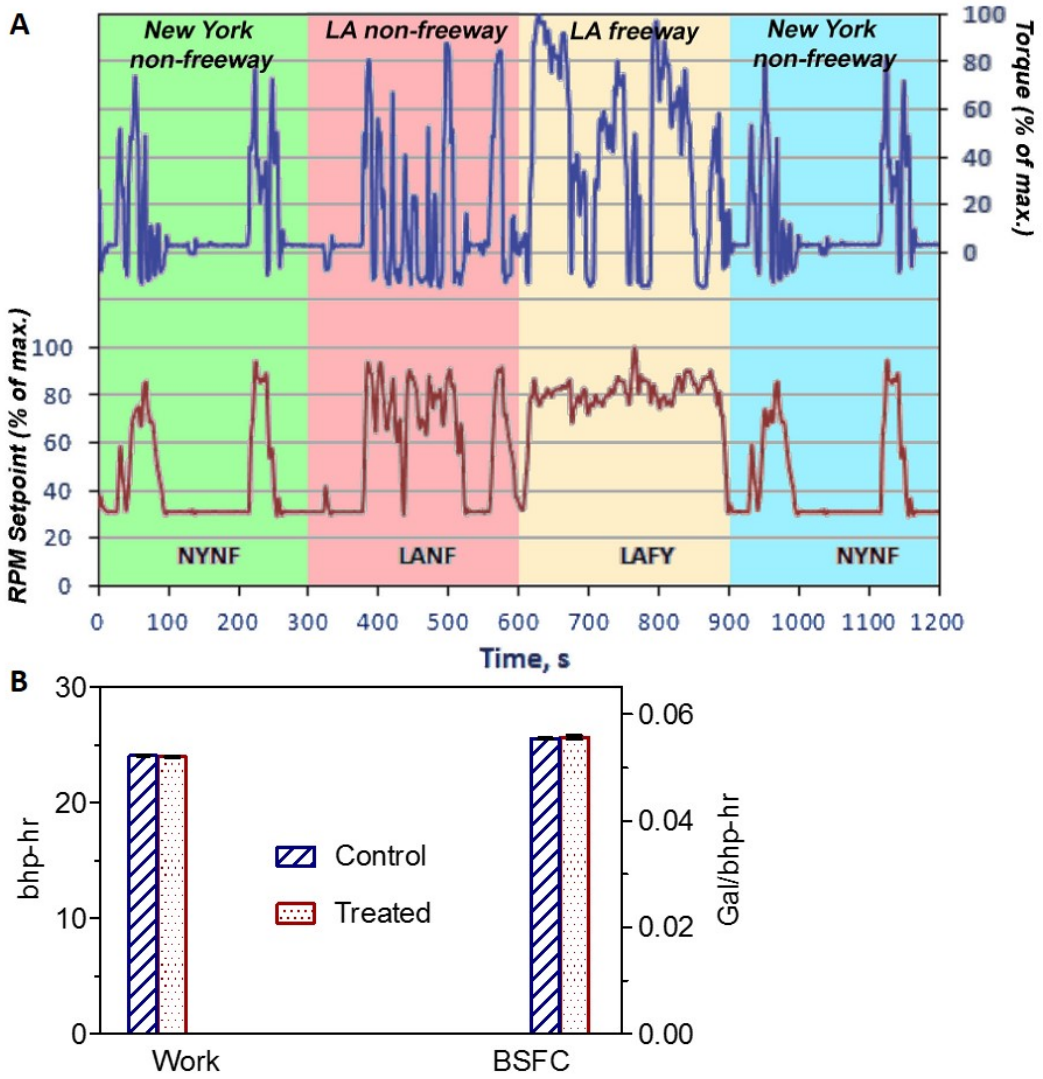

Figure S19

(A) The Federal Test Protocol (FTP) for engine tests is a specified transient of RPM and torque designed to include segments characteristic of two major metropolitan areas in the US. The FTP cycle consists of four phases (300 seconds each): (1) New York Non-Freeway (NYNF, light urban traffic with frequent stops and starts), (2) Los Angeles Non-Freeway (LANF, typical of crowded urban traffic with few stops), (3) Los Angeles Freeway (LAFY, simulating crowded expressway traffic in LA), and (4) a repetition of the first NYNF phase. Initial engine test is performed in double-blind mode, averaging three repetitions of the FTP cycle with all measurements calibrated between each FTP cycle. The test was performed in diesel engines rather than aviation jets due to lack of access to an aviation jet engine test facility. **(B)** Work and fuel efficiency data using an unmodified long-haul diesel engine at the University of California Riverside's Center for Environmental Research and Technology (CE-CERT). Control: untreated diesel. Treated: diesel with 0.14% w/v 670k DA/DB. BSFC: "brake specific fuel consumption" (fuel burned per work done against dynamometer, a parameter for fuel efficiency). Bhp-hr: brake-horsepower-hr (0.746 kW·hr). Gal/bhp-hr: gallons per bhp-hr (5.19 liters / kW·hr).

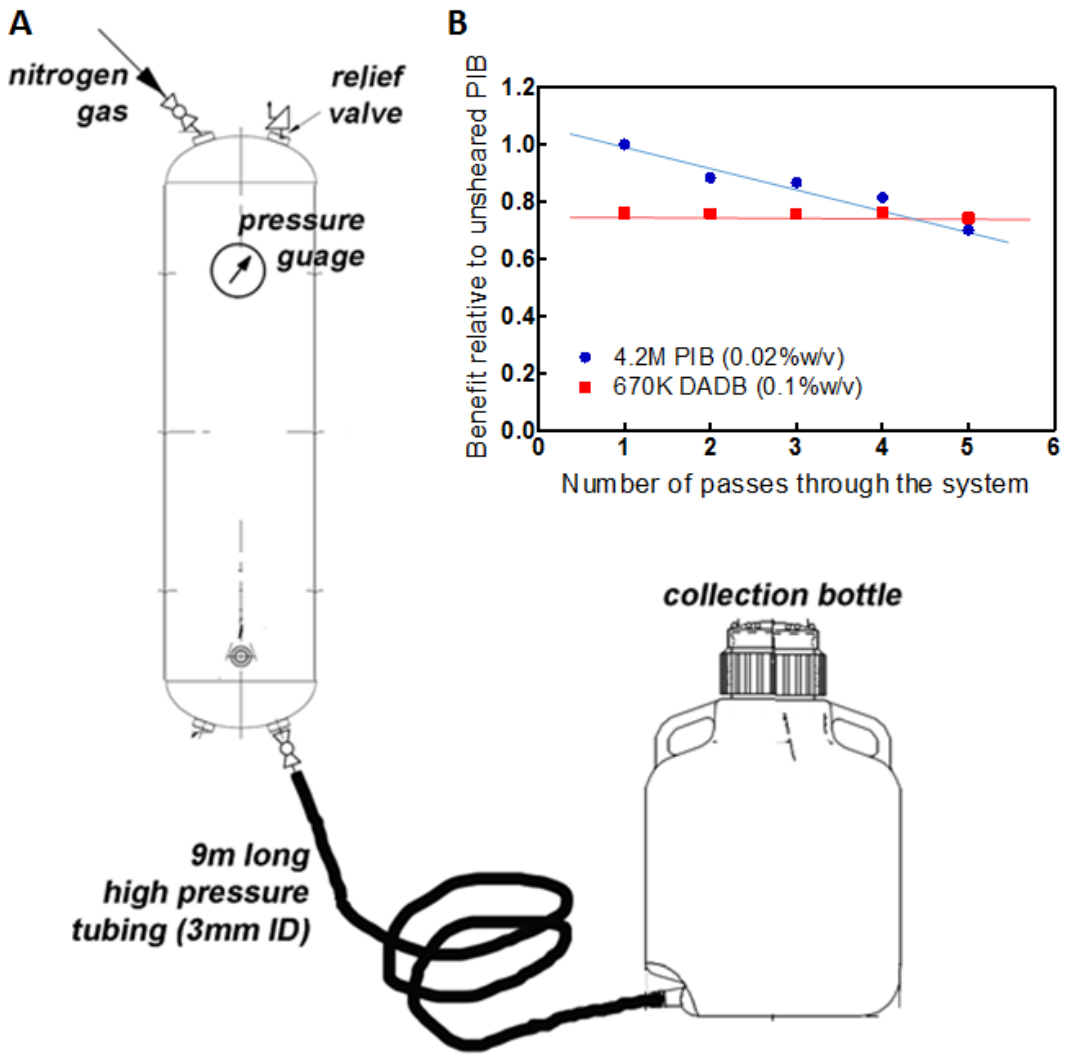

Figure S20

(A) A simple apparatus for drag reduction tests to compare the drag reducing effect of 1:1 molar ratio of α,ω-di(isophthalic acid) polycyclooctadiene and α,ω-di(di(tertiary amine)) polycyclooctadiene mixture (DA/DB, approximately 670 kg/mol) with those of 4.2M PIB: a 2.5-gallon cylindrical tank (Viair 91208, rated to 200 psi) fitted with a pressure gauge, a high-pressure nitrogen supply, a 200-psi relief valve, and a ball valve at the sample outlet, which is connected to a 9.15-meter length of PTFE tubing (I.D. = 3.17 mm, rated to 300psi) and the fuel is collected at ambient pressure in a 10-liter polyethylene (PE) bottle with a tubulation connector at the bottom. Test fluid was pressurized to 200 psi using nitrogen. The time was measured from the time the valve at the bottom of the reservoir was opened to the time the pressure dropped from 200 psi to 192 psi, at which time the valve was closed (less than 22 seconds later). Flow rates were determined by weighing the collection bottle before and after the test. Gravity flow was used to return the test fluid back to the pressure vessel from the 10-liter PE bottle over a period of 35 min (to avoid any degradation). Five passes were performed on each sample. **(B)** Average mass flow rate normalized to that of "as prepared" 4.2M PIB solution for a 0.02% solution of 4.2M PIB in Jet-A and a 0.1% solution of 670k DA/DB in Jet-A (similar to that used in the diesel engine tests of Fig. 3c).

Three types of samples were tested: untreated Jet-A as the control, Jet-A solution of 4.2M PIB at 0.02 % w/v and Jet-A solutions of a 1:1 molar ratio mixture of 670 kg/mol DA/DB (670k DA/DB) at 0.1 % w/v. When untreated Jet-A was tested, a Reynolds number of Re = 10,770 was achieved. The treated samples gave higher Re. Therefore, all experiments were in the turbulent regime in which ultra-long polymers act as drag reducing agents.

The as-prepared solutions in Jet-A show that 670k DA/DB at 0.1% w/v gives an effect that is initially 80% of that of PIB chains of 4.2M PIB at 0.02% w/v. In accord with prior literature, the data show decreasing efficacy of drag reduction by 4.2M PIB with each successive pass through the system—an indication of "shear degradation". The effect of 670k DA/DB does not decrease within 5 passes through the system.

The unprecedented feature of 670k DA/DB is that it gives drag reduction that we do not anticipate to decrease with passage through pumps, fittings or pipelines. Therefore, an effective increase in throughput through a pipeline could conceivably be achieved without requiring re-injection after each pump. In addition, desirable reduction in drag is achieved at a concentration shown to produce improved combustion in a long-haul diesel engine test.

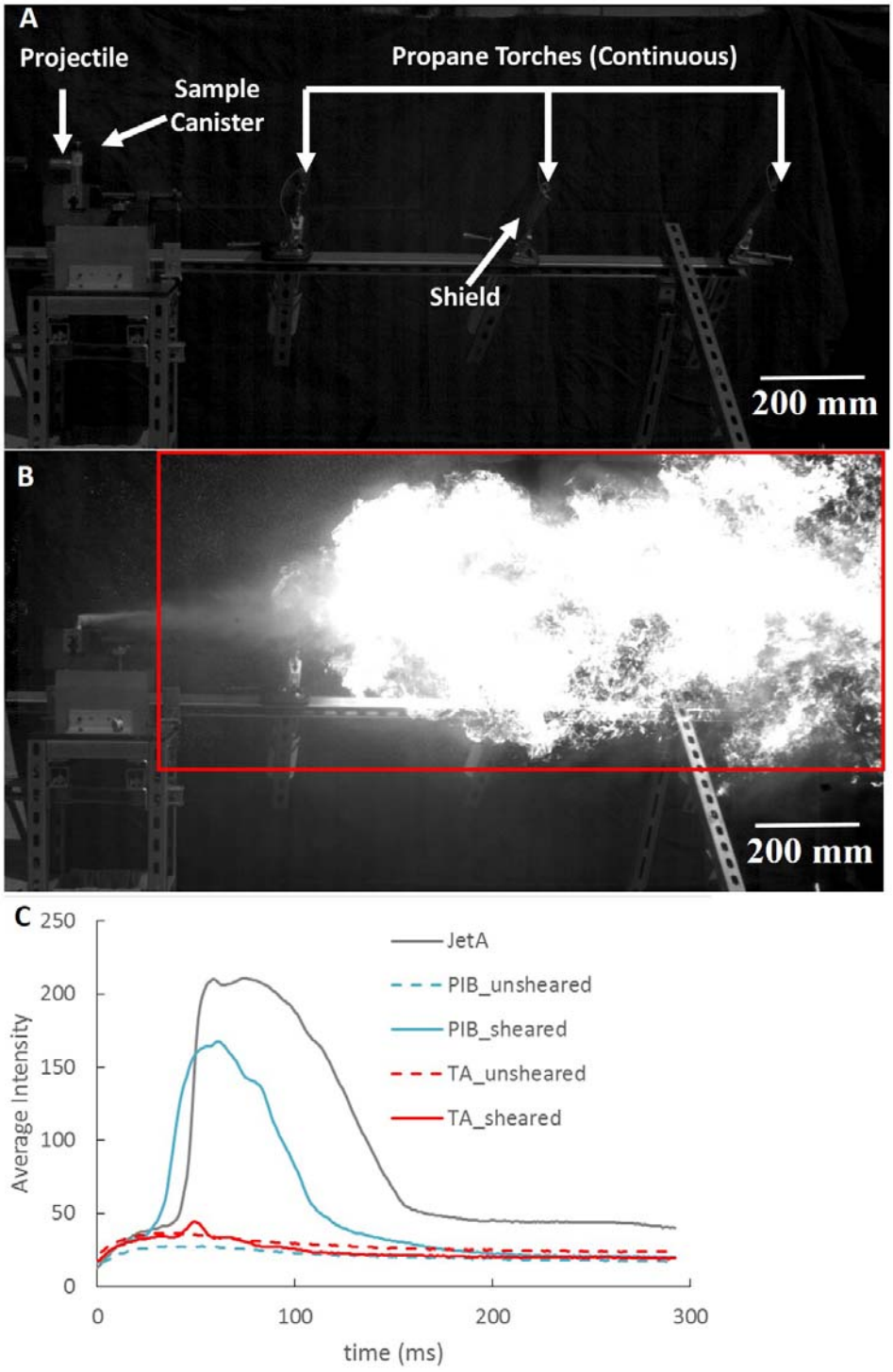

Figure S21

(A) Apparatus for impact/flame propagation experiments. An aluminum canister (outer diameter = 23 mm, height = 100 mm) was used as a miniature fuel tank to hold ~30 mL of a test sample. The cap was tightly sealed with superglue and electrical tape. A stainless steel cylinder (diameter = 24 mm, length = 50 mm) was used as a projectile to impact the sample canister and disperse the fuel. To the left of this image: Compressed air at 6.89×10^5 Pa was used to propel the projectile through a 1.66 m-long barrel (inner diameter = 25.4 mm), resulting in a muzzle speed

of 63 m/s measured by time of flight between two flush-mounted sensors in the barrel. An array of three continuously burning propane torches was placed in the path of the ejected fuel. To prevent the torches from being extinguished by the burst of air from the gun, a shield was placed between the torch tip and the gun. The impact, misting, subsequent ignition and flame propagation were captured using a high-speed camera (Photron SA1.1, frame rate 10 kHz). Image acquisition was triggered by a laser-motion detector attached to the end of muzzle.
(B) Frame at 60.4 ms for untreated Jet-A. The red box is the area within which pixels were analyzed for brightness.
(C) Average brightness of the pixels in the red rectangle of (B) as a function of time during the first 300 ms after impact for five compositions (untreated Jet-A, 0.35 %wt 4.2M PIB unsheared, 0.35 %wt 4.2M PIB sheared, 0.3 %wt 430k TA unsheared and 0.3 %wt 430k TA sheared). The brightness of each pixel was scaled from 0 to 250. The average brightness of the pixels in the red box (shown in part b) was calculated for each frame (every 0.1ms). Untreated Jet-A generated a large fireball (almost all pixels in the red rectangle were saturated) that was relatively long lasting (intense flame from 40ms to 60ms, followed by a prolonged time in which separated flames continued to burn until all fuel was consumed). As-prepared 4.2M PIB suppressed flame propagation (blue dash), but lost its efficacy after the shear treatment described in fig. S18 (solid blue line). 430k TA was effective in mist-control before (red dash) and after (red line) shear.

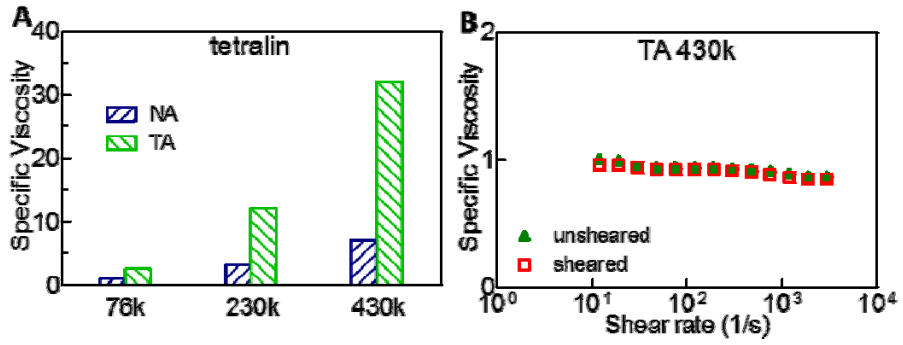

Figure S22

Characterization of α,ω-di(di(isophthalic acid)) (TA) polycyclooctadiene used in Impact test. (A) Effect of chain length (k refers to kg/mol) on specific viscosity of TA in tetralin at 10 mg/ml. **(B)** Specific viscosity of 2.4 mg/ml 430k TA in Jet-A at 25°C, sheared vs unsheared.

The 430k α,ω-di(di(isophthalic acid)) polycyclooctadiene (TA), which is used in the impact test, is self-associative (and might not be pairwise). Although its physics may differ from that of complementary pairs, its rheological properties are similar (**A**), it has similar resistance to shear degradation (**B**) as the α,ω-di(isophthalic acid) polycyclooctadiene and α,ω-di(di(tertiary amine)) polycyclooctadiene 1:1 molar ratio mixture (~670 kg/mol DA/DB), described in the main body text.

Table S3

Molecular design considerations for backbone selection for solubility in fuels and resistance to chain scission.

In contrast to polymers examined in prior literature (*2,9*) on mist control and drag reduction, the present polymers use a backbone that has no tertiary or quaternary carbons nor any heteroatoms in the repeat unit. The importance of these features is illustrated by comparison with the two polymers that have received the most attention in prior literature: 4,200 kg/mol polyisobutylene (PIB) and a copolymer of acrylic and styrenic monomers known as FM-9 (M_w ~ 3,000 kg/mol). Acrylate units introduce heteroatoms that interfere with fuel solubility (a problem that is exacerbated by the random incorporation of carboxylic acid side groups). Polyisobutylene has quaternary carbons in the backbone, making it particularly susceptible to chain scission (*24*). The tertiary backbone carbons in FM-9 also make the backbone more susceptible to chain scission than one that has only secondary carbons. The solubility and strength of the present polymers are enhanced by including carbon-carbon double bonds in the backbone.

Polymer	Solubility in Fuel	E_a of Thermal Backbone Scission (kJ/mol)
4.2M PIB	Excellent	42
FM-9	Very poor	99
Polycyclooctadiene (PCOD)	Excellent	181

PIB: 

FM-9: 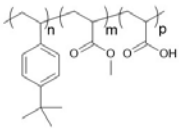

Table S4

Physical properties of single component solvents: Dielectric constant (ε) and refractive index (n).

Dielectric constant serves as a measure of the polarity of solvents: it increases from for cyclohexane (CH) and tetralin. Increasing solvent polarity reduces the degree of end-association for the telechelics.

The difference between the refractive index of solvents and that of PCOD (n ~ 1.52) determines the contrast in multi-angle laser light scattering (MALLS). Tetralin is excluded from the MALLS experiment because of its low contrast with PCOD (1.54 is too close to 1.52). Cyclohexane gives desirable contrast in MALLS.

	Cyclohexane (CH)	Tetralin
Dielectric constant (ε) at 25°C	2.02	2.77
Refractive Index (n) at 20°C	1.426	1.541

Table S5

Preliminary ASTM data of untreated ("Base fuel") and treated JP-8 (with 1:1 molar mixture of 500 kg/mol α,ω-di(isophthalic acid) polycyclooctadiene and 600 kg/mol α,ω-di(di(tertiary amine)) polycyclooctadiene (DA/DB)).

[(a)]The concentration of polymer (mass/mass) added to "Base fuel" JP-8, a military aviation fuel (specified by MIL-DTL-83133), corresponding to Jet-A with three additional additives: the Corrosion Inhibitor/Lubricity Enhancer, the Fuel System Icing Inhibitor, and the Static Dissipater Additive.

[(b)]**Flash Point** (ASTM D93) is the lowest temperature at which fuel will produce enough flammable vapors to ignite when an ignition source is applied. Flash point is the most commonly used property for the evaluation of the flammability hazard of fuels. As expected, the mist-control polymers do not affect the flash point because the polymer additive affects mechanical mist formation—not the liquid-vapor equilibrium characteristics of the fuel. There is no statistically significant difference in flash point among the three samples.

[(c)]**Total Acid Number** (ASTM D3242) organic acids are naturally found in hydrocarbon fuels and others are created during refining. The presence of acids in fuel is unwanted because of the potential to cause corrosions or interfere with fuels water separation. There is no statistically significant difference in total acid number among the three samples.

[(d)] **Density** at -15°C (ASTM D4052) is used to verify fuel type, calculate aircraft fuel load and range, gaging and metering and flow calculations.

[(e)] Kinematic **Viscosity** at -20°C (ASTM D445) at low temperatures is specified to be 8.0mm^2/s or less to ensure adequate fuel flow and atomization under low temperature operations, particularly for engine relight at altitude. The composition at 1000 ppm obeys this criteria.

Property	Base fuel	1000 ppm[(a)]	3000 ppm[(a)]
Flash point[(b)] (ASTM D93)	65.0 °C	64.5 °C	64.5 °C
Acid No.[(c)] (ASTM D3242)	0.004 mgKOH/g	0.003 mgKOH/g	0.004 mgKOH/g
Density[(d)] @15°C (ASTM D4052)	0.8107 kg/L	0.8108 kg/L	0.8109 kg/L
Viscosity[(e)] @-20°C (ASTM D445)	4.8 mm^2/s	6.3 mm^2/s	12.0 mm^2/s

Movie S1
High-speed impact movie for pure Jet-A.

Movie S2
High-speed impact movie for Jet-A treated with 4.2M PIB (0.35% wt) “unsheared”

Movie S3
High-speed impact movie for Jet-A treated with 4.2M PIB (0.35% wt) “sheared”

Movie S4
High-speed impact movie for Jet-A treated with 430k TA (0.3% wt) “unsheared”

Movie S5
High-speed impact movie for Jet-A treated with 430k TA (0.3% wt) “sheared”